Journal of Computational Physics 315 (2016) 16–38

Contents lists available at ScienceDirect

Journal of Computational Physics

www.elsevier.com/locate/jcp

Implicit unified gas-kinetic scheme for steady state solutions in all flow regimes

Yajun Zhu [a], Chengwen Zhong [a], Kun Xu [b,*]

[a] National Key Laboratory of Science and Technology on Aerodynamic Design and Research, Northwestern Polytechnical University, Xi'an, Shaanxi 710072, China

[b] Department of Mathematics, Department of Mechanical and Aerospace Engineering, Hong Kong University of Science and Technology, Hong Kong, China

ARTICLE INFO

Article history:
Received 8 September 2015
Received in revised form 4 February 2016
Accepted 15 March 2016
Available online 21 March 2016

Keywords:
Implicit scheme
Unified gas kinetic scheme
LU-SGS
Steady state solution
Rarefied and continuum flows

ABSTRACT

This paper presents an implicit unified gas-kinetic scheme (UGKS) for non-equilibrium steady state flow computation. The UGKS is a direct modeling method for flow simulation in all regimes with the updates of both macroscopic flow variables and microscopic gas distribution function. By solving the macroscopic equations implicitly, a predicted equilibrium state can be obtained first through iterations. With the newly predicted equilibrium state, the evolution equation of the gas distribution function and the corresponding collision term can be discretized in a fully implicit way for fast convergence through iterations as well. The lower–upper symmetric Gauss–Seidel (LU-SGS) factorization method is implemented to solve both macroscopic and microscopic equations, which improves the efficiency of the scheme. Since the UGKS is a direct modeling method and its physical solution depends on the mesh resolution and the local time step, a physical time step needs to be fixed before using an implicit iterative technique with a pseudo-time marching step. Therefore, the physical time step in the current implicit scheme is determined by the same way as that in the explicit UGKS for capturing the physical solution in all flow regimes, but the convergence to a steady state speeds up through the adoption of a numerical time step with large CFL number. Many numerical test cases in different flow regimes from low speed to hypersonic ones, such as the Couette flow, cavity flow, and the flow passing over a cylinder, are computed to validate the current implicit method. The overall efficiency of the implicit UGKS can be improved by one or two orders of magnitude in comparison with the explicit one.

1. Introduction

The gas-kinetic scheme (GKS) based on the kinetic model equations, such as the Bhatnagar–Gross–Krook (BGK) model [1] of the Boltzmann equation, was proposed by Prendergast and Xu [2,3] for the Euler and high Reynolds number Navier–Stokes (NS) solutions, which has been further developed by Xu [4] for the accurate capturing of low Reynolds number flows as well. The GKS is a robust and accurate scheme for the NS solutions in the smooth region and provides delicate numerical dissipation through particles transport and ineffective collision for the construction of a non-equilibrium numerical shock structure. Since the GKS updates the macroscopic flow variables only and uses the Chapman–Enskog expansion [5] for

* Corresponding author.
E-mail addresses: zhuyajun@mail.nwpu.edu.cn (Y. Zhu), zhongcw@nwpu.edu.cn (C. Zhong), makxu@ust.hk (K. Xu).

http://dx.doi.org/10.1016/j.jcp.2016.03.038
0021-9991/

the construction of a gas distribution function, it is only valid for the continuum flow. In order to extend the scheme for the non-equilibrium flow computation, the gas distribution function itself has to be updated for the capturing of highly non-equilibrium state. With a discretized particle velocity space, a unified gas-kinetic scheme (UGKS) has been constructed for all flow regimes [6,7]. The central ingredient of the UGKS is to use the integral solution of the BGK-type model equation for the gas evolution and the flux evaluation at a cell interface. Due to the multiscale nature of the integral solution, i.e., a time-dependent transition from the kinetic scale particle free transport to the hydrodynamic scale wave propagation, the UGKS can automatically recover flow physics in different regimes with the variation of the ratio between the time step and the local particle collision time. Besides the coupling of particle transport and collision for the gas evolution around a cell interface, this kind of coupling is also necessary for the evaluation of a time-dependent gas distribution function inside each control volume [8]. As a result, the cell size and the time step used in UGKS are not limited by the particle mean free path and mean collision time, and the ratio between the mesh size and particle mean free path can be changed dramatically in different flow regimes. This unified approach provides a promising and general tool for the capturing of multi-scale transport physics, such as rarefied gas dynamics, radiative heat transfer, and plasma evolution [9,10]. In comparison with the direct simulation Monte Carlo (DSMC) method [11] and other discrete velocity methods (DVM) [12–14], the UGKS shows better accuracy and efficiency in the near continuum flow regime. However, in order to make the scheme become a valuable tool in real engineering applications, there is a high demand to develop an implicit UGKS method for fast convergence to the steady state solution, such as in the designs of micro–electro–mechanical system (MEMS) and thermal protection system of spacecrafts. Different from the particle-based DSMC method, there are still discretized governing equations in the UGKS, and the equation-based techniques can be fully utilized for the development of implicit method.

For the GKS, several implicit algorithms have been developed to simulate continuum flow. An early one was based on a simplified gas-kinetic scheme by Chae et al. [15], where alternating direction implicit (ADI) method was applied to solve the implicit equations in multi-dimensional cases. Since the lower–upper symmetric Gauss–Seidel (LU-SGS) factorization method was developed by Yoon and Jameson [16–18], it has been widely used in flow computations [19,20]. The LU-SGS technique has been used in the construction of implicit GKS [21]. Many acceleration techniques, such as local time stepping, multi-grid strategy, and matrix-free LU-SGS iteration have been added into the implicit schemes [22,23]. Moreover, the implicit GKS has also been applied for near continuum flow [22] and with unstructured meshes [24].

For rarefied flow computation, implicit schemes for kinetic model equations with the discretization of gas distribution function can be designed as long as the equilibrium state g^{n+1} in the collision term is known. In Yang and Huang's implicit scheme [25], the equilibrium state g^{n+1} is simply replaced by g^n with an explicit treatment. With a similar treatment, an implicit method for the UGKS has been constructed recently as well [26]. As analyzed by Mieussens [12,13], it may slow down the convergence of an implicit scheme considerably if the gain and loss terms in the kinetic model equations are evaluated at different time levels. The implicit treatment of [26] seems less effective in continuum flow regime and its efficiency may depend sensitively on the numerical tests. Another implicit method for the discrete velocity model is to approximate the equilibrium state g at the next time level [12,13] with a linear mapping between the equilibrium state g and the real gas distribution function f. But, this mapping involves a huge matrix, which increases the complexity of the implicit method. For BGK-type model equation, a moment-based accelerating technique has been developed recently in [27], coupling the kinetic equation and fluid momentum equations.

The present work is to develop an implicit UGKS method, where both macroscopic and microscopic governing equations will be fully coupled in an implicit way. In order to treat the collision term in a fully implicit way, the equilibrium state will be predicted first by solving the macroscopic governing equations implicitly. With the predicted conservative flow variables, the governing equation of the distribution function can be fully discretized implicitly, where a diagonal matrix system about the unknown distribution function will be formed. Then, both matrix systems derived from implicit macroscopic equations and implicit microscopic equation are solved iteratively by using LU-SGS method.

The rest of this paper is organized as follows. In section 2, the explicit UGKS scheme is briefly introduced and the implicit method is presented in details. Section 3 tests the implicit UGKS through the cases of low speed Couette and cavity flows, and high speed flow around a cylinder. The efficiency of the implicit UGKS will be compared with the explicit one and other implicit methods. The last section is the conclusion.

2. Unified gas-kinetic scheme

The UGKS is a direct modeling method for the time evolution of a gas distribution function f in a control volume around space $\vec{x}$, time t, and particle velocity $\vec{u}$,

$$\int_{\Omega} (f(\vec{x},t,\vec{u}) - f_0(\vec{x},\vec{u}))dV + \int_0^t \oint_{\partial\Omega} f\vec{u}\cdot d\vec{S}dt = \int_0^t \int_{\Omega} Q(f,f)dt, \tag{1}$$

where Ω is a control volume in physical space, and $\partial\Omega$ is the boundary of the control volume. The f_0 is the initial gas distribution function at time $t=0$. Here $Q(f,f)$ is the collision term and its effect on the time evolution of f depends on the scale of t. The governing equations for the macroscopic flow variables are based on the modeling equations as well,

$$\int_{\Omega} (\vec{W}(\vec{x},t) - \vec{W}_0(\vec{x}))dV + \int_0^t \oint_{\partial\Omega} \vec{F} dS dt = \vec{0}, \tag{2}$$

where $\vec{W} = [\rho, m, n, \varepsilon]^T = [\rho, \rho U, \rho V, \rho E]^T$ is the vector of conservative flow variables with initial condition $\vec{W}_0$ at $t = 0$, and $\vec{F}$ is a vector of corresponding fluxes. The conservative flow variables can be obtained by taking moments of a gas distribution function

$$\vec{W} = \int f \vec{\psi} d\Xi, \tag{3}$$

where $\vec{\psi} = \left[1, u, v, \frac{1}{2}(u^2 + v^2 + \xi^2)\right]^T$ in a 2D case and $d\Xi = dudvd\xi$. Here ξ represents the random velocities of particle motion in the z-direction for a monatomic gas.

The above two governing equations (1) and (2) are the basic physical conservation laws, which are valid in any scale in the space Ω and time t [7]. The time evolution of a gas distribution function at a cell boundary and the modeling of the collision term Q inside each control volume depend on the scale of the control volume in relative to the scale of particle mean free path and the time in terms of particle collision time. The gas evolution in the control volume (Ω, t) depends critically on the time-dependent solution f at the boundary $\partial\Omega$. With the time increment, the multiple particle collisions make the solution insensitive to the individual binary Boltzmann collision term. As a result, the use of the kinetic model, such as the BGK type equation, i.e., $Q = (g - f)/\tau$, where τ is the relaxation time or mean collision time, and g is the corresponding equilibrium state, can give an accurate description of flow motion in the transition regime, especially in a time scale of $t \geq 2\tau$ [9]. In order to simulate flows with arbitrary Prandtl number Pr in the continuum regime, the Shakhov model [28] is employed in this paper to approximate the equilibrium state g, which has a form of

$$g = g_M \left[1 + (1 - Pr)\vec{c} \cdot \vec{q} \left(\frac{m_0 c^2}{k_B T} - 5\right) \Big/ \left(\frac{5pk_B T}{m_0}\right)\right], \tag{4}$$

where g_M is the Maxwell–Boltzmann distribution, k_B is the Boltzmann constant, m_0 is molecular mass, $\vec{c} = \vec{u} - \vec{U}$ is the peculiar velocity, and $\vec{q}$ is the vector of heat flux.

2.1. Explicit UGKS

As a special application of the general evolution equations (1) and (2), we can choose the cell size V_i as the control volume Ω and the time step $\Delta t = t^{n+1} - t^n$ as the time scale t. Then, the governing equation (1) for the discretized distribution function at particle velocity $\vec{u}_k$ can be expressed as

$$f_{i,k}^{n+1} = f_{i,k}^n - \frac{1}{V_i} \sum_{j \in N(i)} S_{ij} \int_{t^n}^{t^{n+1}} u_{k,n} f_{ij,k}(t) dt + \int_{t^n}^{t^{n+1}} \frac{g_{i,k} - f_{i,k}}{\tau_i} dt, \tag{5}$$

where $N(i)$ is the set of the neighbors of cell i, j is one of the neighboring cell, and ij denotes the interface between cells i and j. In addition, V_i is the volume of the cell i, S_{ij} is the area of the interface ij, $u_{k,n}$ is the normal component of particles velocity $\vec{u}_k$ along the interface, and $f_{ij,k}(t)$ is a time-dependent distribution function on the interface ij at particle velocity $\vec{u}_k$. Similarly, Eq. (2) can be written as

$$\vec{W}_i^{n+1} = \vec{W}_i^n - \frac{1}{V_i} \sum_{j \in N(i)} S_{ij} \left(\sum_k \int_{t^n}^{t^{n+1}} u_{k,n} f_{ij,k}(t) \vec{\psi}_k dt \right), \tag{6}$$

where the fluxes for the conservative flow variables are the moments of the interface gas distribution function as well. Note that both equations (5) and (6) are the basic physical laws in the mesh size and time step scales, which cannot be considered as numerical discretizations of any prescribed governing equation.

In order to evolve the above governing equations, a time-dependent gas distribution function $f_{ij,k}(t)$ on the cell interface has to be modeled. With the time increment, a multiple scale evolution model can be constructed from the integral solution of the BGK-type model,

$$\begin{aligned} f_{ij,k}(t) = f\left(\vec{x}_{ij}, t, \vec{u}_k, \xi\right) = & \frac{1}{\tau} \int_{t^n}^{t} g(\vec{x}', t', \vec{u}_k, \xi) e^{-(t-t')/\tau} dt' \\ & + e^{-(t-t^n)/\tau} f\left(\vec{x}_{ij} - \vec{u}_k\left(t - t^n\right), t^n, \vec{u}_k, \xi\right), \end{aligned} \tag{7}$$

where $\vec{x}' = \vec{x}_{ij} - \vec{u}_k\left(t - t'\right)$ is the trajectory of particle. Eq. (7) is derived from the assumption that τ is a local constant, which is fully determined from the local macroscopic variables,

$$\tau = \frac{\mu}{p},$$

where μ is the dynamic viscosity coefficient and p is the pressure. Eq. (7) is a multiscale modeling of gas evolution from the kinetic scale particle free transport to the hydrodynamic scale equilibrium formation. This evolution model is the key for the closure of the multiple scale governing equations (5) and (6). In Eq. (7), the initial distribution function around the cell interface can be constructed as

$$f_{0,k}(\vec{x}) = f(\vec{x}, t^n, \vec{u}_k, \xi) = \begin{cases} f^i_{ij,k} + (f_{\vec{x}})^n_i \cdot \vec{x}, & \vec{n}_{ij} \cdot \vec{x} < 0, \\ f^j_{ij,k} + (f_{\vec{x}})^n_j \cdot \vec{x}, & \vec{n}_{ij} \cdot \vec{x} \geq 0, \end{cases}$$

where $f^i_{ij,k}$ and $f^j_{ij,k}$ are the initial distribution functions at both sides of the cell interface ij respectively, and $\vec{n}_{ij}$ is the unit normal vector of the interface pointing from cell i to cell j. Here $f_{\vec{x}}$ is the spatial gradient of the initial distribution function f_0. The equilibrium distribution function g has the distribution in space and time

$$g(\vec{x}, t) = g_0 + g_{\vec{x}} \cdot \vec{x} + g_t t,$$

where g_0 is the equilibrium state at the interface ij obtained from initial distribution function f_0, $g_{\vec{x}}$ and g_t are the spatial and temporal gradients of the equilibrium state g_0. More detailed descriptions of f_0, g_0, $f_{\vec{x}}$, $g_{\vec{x}}$, and g_t can be found in [6,7,29]. Then the corresponding fluxes across the interface during a time step Δt can be computed by

$$\int_0^{\Delta t} u_{k,n} f_{ij,k}(t) dt = u_{k,n}\left(q_1 g_0 + q_2 \vec{u}_k \cdot g_{\vec{x}} + q_3 g_t\right) + u_{k,n}\left(q_4 f_0 + q_5 \vec{u}_k \cdot f_{\vec{x}}\right),$$

where the coefficients q are defined as

$$\begin{aligned} q_1 &= \tau\left[\tau_0 - \left(1 - e^{-\tau_0}\right)\right], \\ q_2 &= \tau^2\left[-\tau_0 - \tau_0 e^{-\tau_0} + 2\left(1 - e^{-\tau_0}\right)\right], \\ q_3 &= \tau^2\left[\frac{1}{2}\tau_0^2 - \tau_0 + \left(1 - e^{-\tau_0}\right)\right], \\ q_4 &= \tau\left(1 - e^{-\tau_0}\right), \\ q_5 &= \tau^2\left[\tau_0 e^{-\tau_0} - \left(1 - e^{-\tau_0}\right)\right], \end{aligned}$$

where τ is the cell interface particle collision time and $\tau_0 = \Delta t/\tau$.

For the explicit UGKS, as long as the distribution function $f_{ij,k}(t)$ is obtained, the fluxes for the gas distribution function and the conservative flow variables can be evaluated. With the updated conservative flow variables in Eq. (6), the equilibrium state g^{n+1} can be determined. In the explicit UGKS for unsteady flows, the collision term in Eq. (5) can be approximated by the trapezoidal rule for a second-order scheme in time, i.e.,

$$\int_{t^n}^{t^{n+1}} \frac{g_{i,k} - f_{i,k}}{\tau_i} dt = \frac{\Delta t}{2}\left(\frac{g^n_{i,k} - f^n_{i,k}}{\tau^n_i} + \frac{g^{n+1}_{i,k} - f^{n+1}_{i,k}}{\tau^{n+1}_i}\right),$$

and the gas distribution function $f^{n+1}_{i,k}$ can be updated through Eq. (5). The above explicit scheme has second order accuracy in space and time. The results from the explicit UGKS will be used for comparison with the results from the implicit method. Indeed, for the steady state solutions, using $\Delta t(g^{n+1}_{i,k} - f^{n+1}_{i,k})/\tau^{n+1}_i$ to approximate the collision term is sufficient.

In Eq. (7), the time-dependent distribution function $f_{ij,k}(t)$ is constructed from the local information in cell i and cell j, and an appropriate time scale t should be chosen to keep the gas evolution consistent with physical space resolution. For the explicit UGKS, the time step is always determined by the stability condition,

$$\Delta t_p = \mathrm{CFL} \cdot \frac{\min \Delta l}{\max|\vec{u}_k|}, \tag{8}$$

where Δl is the mesh size and the CFL number is less than one. The CFL condition is not only a necessary condition for stability, but also provides a scale to identify the flow physics. Since the evolution solution depends on τ_0, the explicit time step Δt can represent different flow physics, such as the hydrodynamic scale ($\tau_0 \gg 1$) and the transition one ($\tau_0 \approx 1$). Therefore, the above CFL condition-based time step is denoted by Δt_p as the physical time step, which is distinguishable from a large numerical time step Δt used later in an implicit scheme. Since the numerical time step is for the convergence of the steady state solution only, it has no any direct connection with the physical time step. For the UGKS, the above physical time step Δt_p should be retained for the flux evaluation in order to capture the correct physical solution.

2.2. Implicit UGKS

For steady state calculation, the implicit method is usually developed by discretizing Eq. (5) at time t^{n+1} by a backward Euler method,

$$\frac{V_i}{\Delta t}\left(f_{i,k}^{n+1}-f_{i,k}^{n}\right)+\sum_{j\in N(i)}S_{ij}u_{k,n}f_{ij,k}^{n+1}=V_i\frac{g_{i,k}^{n+1}-f_{i,k}^{n+1}}{\tau_i^{n+1}}.$$

In the above equation, the term of g^{n+1} should be approximated first. As mentioned in the introduction section, one of the choices is to approximate it directly using g^n. Another choice is to linearize it with $g^{n+1}=g^n+\mathbf{M}\cdot\left(f^{n+1}-f^n\right)$ in the velocity space [12,13], where $\mathbf{M}$ is a $K\times K$ matrix and K is the total number of discrete velocities. The former one is very easy to implement, but is associated with slow convergence. The latter one performs better in convergence, but it involves complexities of computation. Different from the above approaches, due to the use of macroscopic governing equations in UGKS, a prediction step can be done first for the update of conservative flow variables and the evaluation of the equilibrium state $\tilde{g}^{n+1}$, before solving the microscopic governing equation implicitly.

2.2.1. Prediction step for approximating equilibrium state

Discretizing Eq. (6) at time t^{n+1} by a backward Euler method, the implicit macroscopic governing equations become

$$\frac{V_i}{\Delta t}\left(\tilde{\vec{W}}_i^{n+1}-\vec{W}_i^{n}\right)+\sum_{j\in N(i)}S_{ij}\vec{F}_{ij}^{n+1}=\vec{0},$$

where $\tilde{\vec{W}}_i^{n+1}$ are the conservative variables to be predicted. Subtracting the fluxes at time t^n from both sides, the governing equations could be rewritten in delta-form as

$$\frac{V_i}{\Delta t}\Delta\vec{W}_i^{n+1}+\sum_{j\in N(i)}S_{ij}\Delta\vec{F}_{ij}^{n+1}=-\sum_{j\in N(i)}S_{ij}\vec{F}_{ij}^{n}, \tag{9}$$

where $\Delta\vec{W}_i^{n+1}=\tilde{\vec{W}}_i^{n+1}-\vec{W}_i^{n}$ and $\Delta\vec{F}_{ij}^{n+1}=\vec{F}_{ij}^{n+1}-\vec{F}_{ij}^{n}$.

At the steady state, the Δ-quantities in Eq. (9) go to zero, and the physical solution will be completely controlled by

$$\sum_{j\in N(i)}S_{ij}\vec{F}_{ij}^{n}=\sum_{j\in N(i)}S_{ij}\left(\frac{1}{t}\sum_k\int_0^t u_{k,n}f_{ij,k}(t')\vec{\psi}_k dt'\right)=\vec{0},$$

which is the macroscopic governing equation for steady state solutions. Since the flow physics in UGKS is closely related to the time step, in order to ensure that the implicit scheme is able to capture multiple scale UGKS solution, an appropriate time scale t should be chosen to calculate the macroscopic fluxes. Therefore, a physical time step Δt_p in Eq. (8) will be used to determine the time-averaged fluxes on the right hand side of Eq. (9), which are defined as the residuals,

$$\vec{R}_i^n=-\frac{1}{V_i}\sum_{j\in N(i)}S_{ij}\vec{F}_{ij}^{n}=-\frac{1}{V_i}\sum_{j\in N(i)}S_{ij}\left(\frac{1}{\Delta t_p}\sum_k\int_0^{\Delta t_p}u_{k,n}f_{ij,k}(t)\vec{\psi}_k dt\right). \tag{10}$$

Certainly, this approach has already been used before in the construction of the implicit gas-kinetic schemes [21,22,24]. Once the residuals go to zero, the implicit UGKS is supposed to converge to the same steady state solution of the explicit UGKS. In the implicit UGKS, the numerical time step Δt is different from the physical one Δt_p, and the numerical one can take a value as large as possible, as long as the implicit scheme is stable. In addition, the discretization of the terms on the left hand side of Eq. (9) will not affect the final convergent solution.

In order to reduce computational cost, the implicit flux $\Delta\vec{F}_{ij}^{n+1}$ is approximated by the Euler equations-based flux splitting method for developing a matrix-free algorithm,

$$\Delta\vec{F}_{ij}^{n+1}=\frac{1}{2}\left[\Delta\vec{T}_i^{n+1}+\Delta\vec{T}_j^{n+1}+r_{ij}\left(\Delta\vec{W}_i^{n+1}-\Delta\vec{W}_j^{n+1}\right)\right]. \tag{11}$$

Here $\vec{T}$ is the Euler flux, which is a function of conservative variables

$$\vec{T}=\cos\theta\cdot\vec{T}_x+\sin\theta\cdot\vec{T}_y,$$

$$\vec{T}_x=\left[m,\frac{m^2}{\rho}+p,\frac{mn}{\rho},\frac{m}{\rho}(\varepsilon+p)\right]^T,$$

$$\vec{T}_y=\left[n,\frac{mn}{\rho},\frac{n^2}{\rho}+p,\frac{n}{\rho}(\varepsilon+p)\right]^T,$$

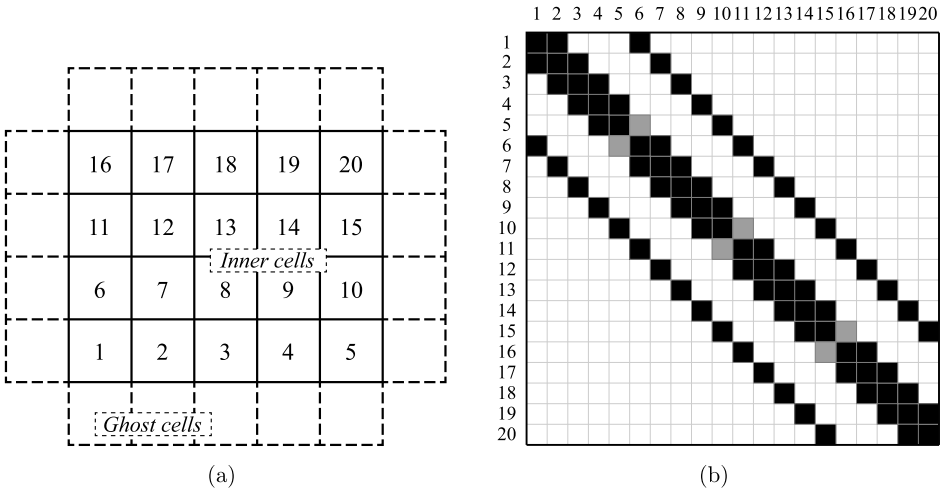

Fig. 1. (a) Index of discrete finite-volume cells; (b) penta-diagonal matrix, the black squares represent the information of inner cells, and the grey ones represent the information of ghost cells.

and the pressure p is

$$p = (\gamma - 1)\left(\varepsilon - \frac{m^2 + n^2}{2\rho}\right).$$

The factor r_{ij} satisfies

$$r_{ij} \geq \Lambda_{ij} = \left|\vec{U}_{ij} \cdot \vec{n}_{ij}\right| + a_s,$$

to ensure a diagonal dominant matrix system, where Λ_{ij} represents the spectral radius of the Euler flux Jacobian, which can be determined by the velocity $\vec{U}_{ij}$ and the speed of sound a_s at the interface ij, and the normal vector of interface $\vec{n}_{ij} = [\cos\theta, \sin\theta]^T$ along the direction from cell i to cell j. With an over-relaxation parameter ϖ [30,31], r_{ij} has a form of $r_{ij} = \varpi\,\Lambda_{ij}$, where $1 \leq \varpi \leq 2$. Stability and convergence can be controlled by adjusting ϖ either manually or automatically. In some implicit schemes [22,32], a stable factor s_{ij} related to the viscosity coefficient is introduced in the computation of r_{ij}, such as

$$r_{ij} = \Lambda_{ij} + s_{ij} = \Lambda_{ij} + 2\nu/\Delta l, \tag{12}$$

which increases the stability of the implicit scheme.

Since the relationship $\sum_{j\in N(i)} S_{ij}\Delta\vec{T}_i^{n+1} = \vec{0}$ is always satisfied for any closed finite volume i in a steady state solution, substituting Eq. (11) into Eq. (9), the governing equation for the conservative flow variables can be simplified as

$$\left(\frac{V_i}{\Delta t} + \frac{1}{2}\sum_{j\in N(i)} S_{ij} r_{ij}\right)\Delta\vec{W}_i^{n+1} + \frac{1}{2}\sum_{j\in N(i)} S_{ij}\left[\vec{T}(\tilde{\vec{W}}_j^{n+1}) - \vec{T}(\vec{W}_j^{n}) - r_{ij}\Delta\vec{W}_j^{n+1}\right] = -\sum_{j\in N(i)} S_{ij}\vec{F}_{ij}^{n}. \tag{13}$$

When Eq. (13) is solved in a finite volume mesh with indexes shown in Fig. 1(a), in two dimensional case a block penta-diagonal matrix as illustrated in Fig. 1(b) can be obtained. If the inverse matrix is obtained, $\tilde{\vec{W}}_i^{n+1}$ could be easily updated. However, it is too expensive to get the inverse of this large sparse matrix directly. Thus, the LU-SGS technique based on LU factorization and Gauss–Seidel iterations can be employed. The matrix system obtained from Eq. (13) can be written as

$$(\mathbf{L} + \mathbf{D} + \mathbf{U}) \cdot \vec{X} = \vec{Y},$$

where $\mathbf{L}$ is a strictly lower triangular matrix, $\mathbf{U}$ is a strictly upper triangular matrix, and $\mathbf{D}$ is a diagonal matrix. With LU factorization, dropping the terms of second orders, it can be approximated as

$$(\mathbf{L} + \mathbf{D})\,\mathbf{D}^{-1}\,(\mathbf{D} + \mathbf{U}) \cdot \vec{X} \approx \vec{Y}.$$

Then it can be solved in two steps, i.e., a forward sweep step

$$(\mathbf{L} + \mathbf{D}) \cdot \vec{X}^{\star} = \vec{Y}, \tag{14}$$

and a backward sweep step

$$\vec{X} = \vec{X}^{\star} - \mathbf{D}^{-1}\mathbf{U}\cdot\vec{X}. \tag{15}$$

During the forward sweep step, only the cells in the lower triangular matrix are involved and form a tri-diagonal matrix. A Gauss–Seidel iteration process can be applied to solve this tri-diagonal matrix. Similarly, the backward sweep step can be easily implemented. With Eq. (14) and (15), Eq. (13) can be solved iteratively by a forward sweep step

$$\left(\frac{V_i}{\Delta t} + \frac{1}{2}\sum_{j\in N(i)} S_{ij}r_{ij}\right)\Delta\vec{W}_i^{\star} + \frac{1}{2}\sum_{j\in L(i)} S_{ij}\left[\vec{T}(\vec{W}_j^n + \Delta\vec{W}_j^{\star}) - \vec{T}(\vec{W}_j^n) - r_{ij}\Delta\vec{W}_j^{\star}\right] = V_i\vec{R}_i^n, \tag{16}$$

and a backward sweep step

$$\begin{aligned}&\left(\frac{V_i}{\Delta t} + \frac{1}{2}\sum_{j\in N(i)} S_{ij}r_{ij}\right)\Delta\vec{W}_i^{n+1} + \frac{1}{2}\sum_{j\in U(i)} S_{ij}\left[\vec{T}(\vec{W}_j^n + \Delta\vec{W}_j^{n+1}) - \vec{T}(\vec{W}_j^n) - r_{ij}\Delta\vec{W}_j^{n+1}\right]\\ &= \left(\frac{V_i}{\Delta t} + \frac{1}{2}\sum_{j\in N(i)} S_{ij}r_{ij}\right)\Delta\vec{W}_i^{\star},\end{aligned} \tag{17}$$

where $L(i)$ and $U(i)$ are subsets of $N(i)$, and $L(i)$ is the neighboring cells of cell i occupying in the lower triangular area of this matrix, and $U(i)$ is the ones in the upper triangular area.

Besides the original LU-SGS iteration method in Eq. (14) and Eq. (15), there is another iteration method which is called point relaxation scheme [33,34]. The point relaxation scheme takes into account the most recently calculated non-main block diagonal values to update the main block diagonals. This can be done for each inner cell by sweeping sequentially through the computational domain. But, unlike the original LU-SGS, the forward step and backward step can be done for several times until a satisfactory solution is obtained. Though more inner iterations take more CPU time, it will still get a better efficiency for convergence than the original one. If a forward sweep plus a backward sweep counts as one sweep denoted by PR(1), then the m-th sweep could be implemented by a forward sweep step

$$\begin{aligned}&\left(\frac{V_i}{\Delta t} + \frac{1}{2}\sum_{j\in N(i)} S_{ij}r_{ij}\right)\Delta\vec{W}_i^{\star} + \frac{1}{2}\sum_{j\in L(i)} S_{ij}\left[\vec{T}(\vec{W}_j^n + \Delta\vec{W}_j^{\star}) - \vec{T}(\vec{W}_j^n) - r_{ij}\Delta\vec{W}_j^{\star}\right]\\ &+ \frac{1}{2}\sum_{j\in U(i)} S_{ij}\left[\vec{T}(\vec{W}_j^n + \Delta\vec{W}_j^{m-1}) - \vec{T}(\vec{W}_j^n) - r_{ij}\Delta\vec{W}_j^{m-1}\right] = V_i\vec{R}_i^n,\end{aligned} \tag{18}$$

followed by a backward sweep step

$$\begin{aligned}&\left(\frac{V_i}{\Delta t} + \frac{1}{2}\sum_{j\in N(i)} S_{ij}r_{ij}\right)\Delta\vec{W}_i^{m} + \frac{1}{2}\sum_{j\in L(i)} S_{ij}\left[\vec{T}(\vec{W}_j^n + \Delta\vec{W}_j^{\star}) - \vec{T}(\vec{W}_j^n) - r_{ij}\Delta\vec{W}_j^{\star}\right]\\ &+ \frac{1}{2}\sum_{j\in U(i)} S_{ij}\left[\vec{T}(\vec{W}_j^n + \Delta\vec{W}_j^{m}) - \vec{T}(\vec{W}_j^n) - r_{ij}\Delta\vec{W}_j^{m}\right] = V_i\vec{R}_i^n,\end{aligned} \tag{19}$$

where $\Delta\vec{W}_i^{m-1}$ is the result from the $(m-1)$-th inner iteration, and $\Delta\vec{W}_i^{\star}$ is the temporary result of the forward step in the m-th inner iteration. After the backward sweep in the m-th sweep, the result $\Delta\vec{W}_i^{m}$ will be obtained. It is found that PR(2) is optimum in all PR(m) [34]. Therefore, PR(2) is chosen to solve the implicit conservation equations in this prediction step. The efficiency of the original LU-SGS method and PR(2) scheme will be tested and compared with each other in Section 3. Once the conservative flow variables are obtained, the equilibrium state $\tilde{g}^{n+1}$ is known in the Shakhov model.

2.2.2. Evolution step for updating particle distribution function

With the predicted equilibrium state $\tilde{g}^{n+1}$, the governing equation of distribution function can be discretized in a fully implicit way by a backward Euler method,

$$\frac{V_i}{\Delta t}\left(f_{i,k}^{n+1} - f_{i,k}^{n}\right) + \sum_{j\in N(i)} u_{k,n}S_{ij}f_{ij,k}^{n+1} = V_i\frac{\tilde{g}_{i,k}^{n+1} - f_{i,k}^{n+1}}{\tilde{\tau}_i^{n+1}},$$

which can be rewritten in a delta-form,

$$\left(\frac{V_i}{\Delta t} + \frac{V_i}{\tilde{\tau}_i^{n+1}}\right)\Delta f_{i,k}^{n+1} + \sum_{j\in N(i)} u_{k,n}S_{ij}\Delta f_{ij,k}^{n+1} = V_i\frac{\tilde{g}_{i,k}^{n+1} - f_{i,k}^{n}}{\tilde{\tau}_i^{n+1}} - \sum_{j\in N(i)} S_{ij}u_{k,n}f_{ij,k}^{n}. \tag{20}$$

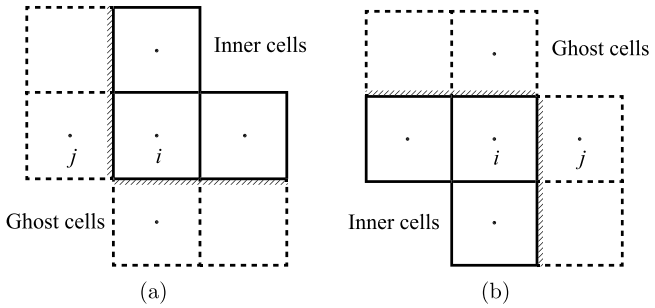

Fig. 2. Ghost cells for boundary conditions. (a) Ghost cell $j \in L_{gc}$; (b) ghost cell $j \in U_{gc}$.

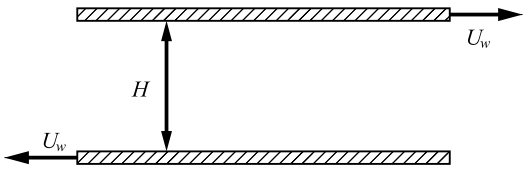

Fig. 3. Illustration of the Couette flow.

Table 1
Acceleration rate of the implicit UGKS and mass loss for the Couette flow in different flow regimes. The acceleration rate is defined as the CPU time ratio of the explicit UGKS to the implicit scheme.

Knudsen number	Acceleration rate	Mass loss (%)
$20/\sqrt{\pi}$	351.11	0.002
$2/\sqrt{\pi}$	198.75	0.015
$0.2/\sqrt{\pi}$	53.10	0.029
0.01	19.49	−0.007
10^{-4}	35.78	−0.107

Since different algorithms to compute the implicit fluxes in delta-forms will not effect the final convergent solution, the distribution function on the cell interface ij on the left hand side of the above equation will be constructed by the upwind scheme

$$\begin{aligned}\Delta f_{ij,k}^{n+1} &= \frac{1}{2}\left(\Delta f_{i,k}^{n+1} + \Delta f_{j,k}^{n+1}\right) + \frac{1}{2}\text{sign}(\vec{u}_k \cdot \vec{n}_{ij})\left(\Delta f_{i,k}^{n+1} - \Delta f_{j,k}^{n+1}\right) \\ &= \frac{1}{2}\left[1 + \text{sign}(u_{k,n})\right]\Delta f_{i,k}^{n+1} + \frac{1}{2}\left[1 - \text{sign}(u_{k,n})\right]\Delta f_{j,k}^{n+1}. \end{aligned} \tag{21}$$

Similarly, for the implicit scheme to converge to the same solution as that of the explicit UGKS, the explicit fluxes on the right hand side of Eq. (20) are computed by the explicit UGKS over a physical time step Δt_p,

$$\sum_{j\in N(i)} u_{k,n} S_{ij} f_{ij,k}^{n} = \frac{1}{\Delta t_p}\sum_{j\in N(i)} \int_0^{\Delta t_p} u_{k,n} S_{ij} f_{ij,k}(t) dt.$$

Then, the final expression of Eq. (20) has a form of

$$D_{i,k}\Delta f_{i,k}^{n+1} + \sum_{j\in N(i)} D_{j,k}\Delta f_{j,k}^{n+1} = \text{RHS}, \tag{22}$$

where

$$\begin{aligned} D_{i,k} &= \frac{V_i}{\Delta t} + \frac{V_i}{\tilde{\tau}_i^{n+1}} + \frac{1}{2}\sum_{j\in N(i)} u_{k,n} S_{ij}\left[1 + \text{sign}(u_{k,n})\right], \\ D_{j,k} &= \frac{1}{2} u_{k,n} S_{ij}\left[1 - \text{sign}(u_{k,n})\right], \\ \text{RHS} &= V_i \frac{\tilde{g}_{i,k}^{n+1} - f_{i,k}^{n}}{\tilde{\tau}_i^{n+1}} - \sum_{j\in N(i)} S_{ij} u_{k,n} f_{ij,k}^{n}. \end{aligned} \tag{23}$$

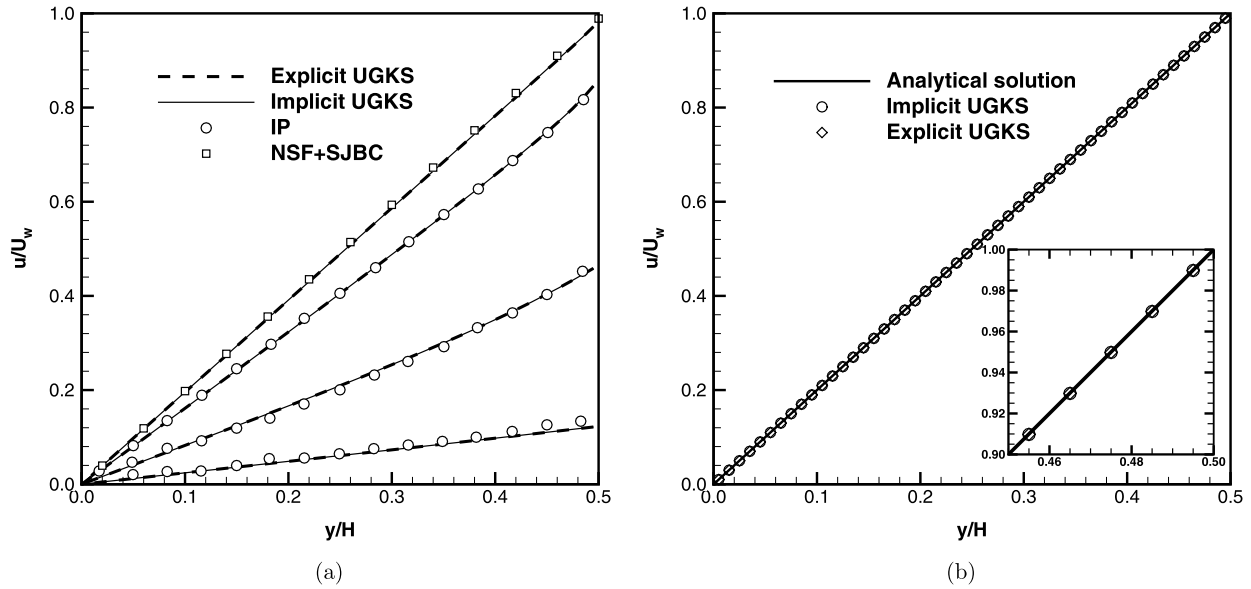

Fig. 4. Velocity along y-direction in the Couette flow. (a) The Couette flow at $\mathrm{Kn} = 0.01, 0.2/\sqrt{\pi}, 2.0/\sqrt{\pi}$ and $20/\sqrt{\pi}$. Solid line: implicit UGKS, dashed line: explicit UGKS, circle: IP method from [37], square: Navier–Stokes and Fourier solution from [38]. (b) The Couette flow at $\mathrm{Kn} = 10^{-4}$. Solid line: analytical solution for the Couette flow in continuum limit with non-slip boundary condition, diamond: explicit UGKS, circle: implicit UGKS.

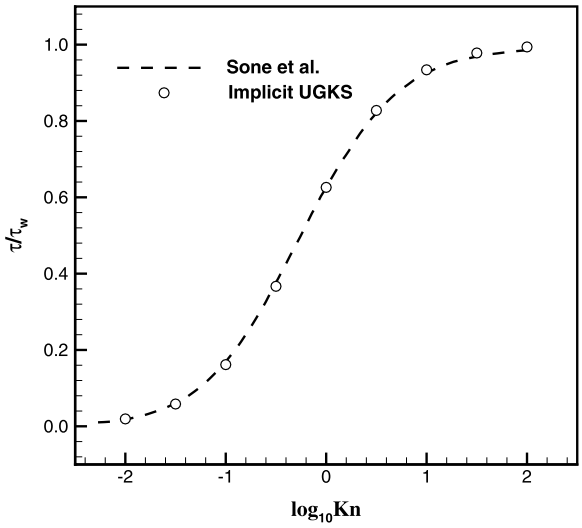

Fig. 5. Stress of the Couette flows with respect to Knudsen number. Circle: results of implicit UGKS, dashed line: data in paper [39].

These terms $D_{i,k}$ and $D_{j,k}$ will be the diagonal entries of a penta-diagonal matrix. Once the steady state is reached, $\Delta f_{i,k}^{n+1}$ and $\Delta f_{j,k}^{n+1}$ will go to zero, and RHS in Eq. (22) should be zero as well. The RHS in Eq. (23) shows that the UGKS couples both transport and collision process in the gas evolution at the cell interface and inside the cell. For the steady state solution, the net flux of gas distribution function at a specific particle velocity around a closed cell boundary is not zero, which is balanced by the particle scattering in and out of this particle velocity $\vec{u}_k$ within the cell.

After applying the standard LU-SGS technique in Eq. (14) and (15) to solve Eq. (22), the distribution function is updated by a forward sweep step

$$D_{i,k}\Delta f_{i,k}^{\star} + \sum_{j\in L(i)} D_{j,k}\Delta f_{j,k}^{\star} = \mathrm{RHS}, \tag{24}$$

followed by a backward sweep step

$$\Delta f_{i,k}^{n+1} = \Delta f_{i,k}^{\star} - D_{i,k}^{-1} \cdot \sum_{j\in U(i)} D_{j,k}\Delta f_{j,k}^{n+1}. \tag{25}$$

Table 2
Iteration steps, total CPU time, and mass loss for the Couette flow at Kn = 0.01 from different prediction step of iterative methods.

Iteration method	CFL	Iteration steps	CPU costs (sec)	Mass loss (%)
Reference scheme[a]	10	20722	1544.9	0.02320
	10^2	13604	1013.3	0.02426
	10^3	12892	960.7	0.02443
	10^4	12821	954.9	0.02444
	10^{10}	12813	954.4	0.02445
Implicit UGKS (A)	10	13067	1120.2	−0.0310
	10^2	7042	598.4	−0.1353
	10^3	6463	548.3	−0.1580
	10^4	6406	543.7	−0.1605
	10^{10}	6400	543.2	−0.1608
Implicit UGKS (B)	10	8813	747.3	−0.0128
	10^2	4207	356.8	−0.1605
	10^3	3766	319.8	−0.2003
	10^4	3722	315.9	−0.2048
	10^{10}	3717	315.6	−0.2053

[a] The prediction step is skipped, where $\tilde{g}^{n+1}$ is simply approximated by g^n.

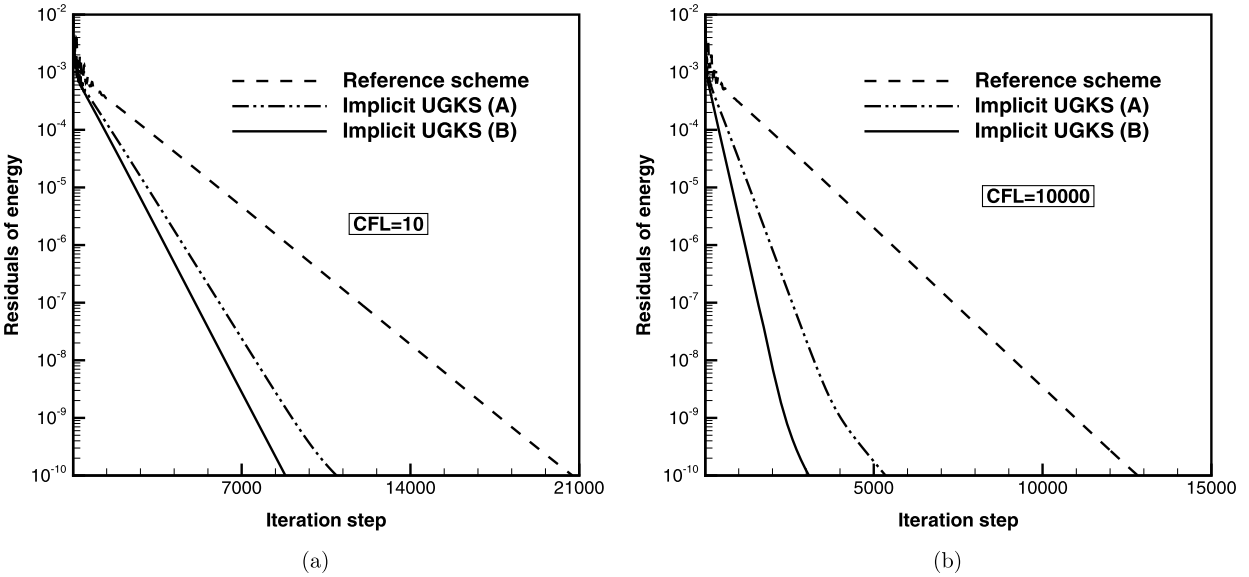

Fig. 6. The convergence histories of the residual for the Couette flow at Kn = 0.01 from different iteration methods. (a) CFL = 10; (b) CFL = 10000.

After getting f^{n+1}, the conservative flow variables $\vec{W}^{n+1}$ can be easily obtained by Eq. (3).

At end, the major steps of the implicit method can be summarized as follows.

Step 1. Start the computation with an initialized flow field, where the gas distribution functions in each cell are Maxwellian.

Step 2. Calculate the time-averaged fluxes over a physical time step Δt_p and evaluate the residuals $\vec{R}_i^n$ by Eq. (10). The residuals are calculated with a second-order accuracy by the gas evolution process in Eq. (7).

Step 3. Solve the implicit macroscopic equations Eq. (13) to predict the conservative variables $\tilde{\vec{W}}^{n+1}$. Eq. (13) can be iteratively solved by adopting a standard LU-SGS sweep process in Eq. (16) and (17), or a point relaxation scheme in Eq. (18) and (19). With the predicted conservative flow variables $\tilde{\vec{W}}^{n+1}$, the equilibrium state $\tilde{g}^{n+1}$ can be obtained in the Shakhov model (4).

Step 4. Solve the microscopic equation (20) implicitly using the LU-SGS method in Eq. (24) and (25) for f^{n+1}.

Step 5. Take moments of distribution function f^{n+1} to obtain macroscopic flow variables, such as density, velocity, pressure, stress and heat flux; and update the equilibrium state g^{n+1}.

Step 6. Go to Step 2 if the residuals do not satisfy the convergent condition. Otherwise, output the flow field and stop the computation.

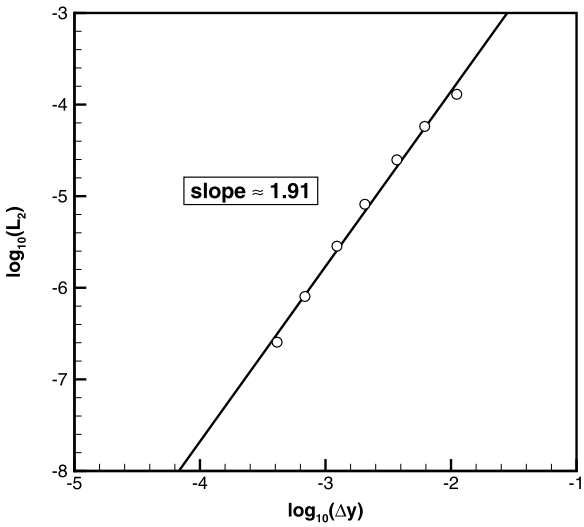

Fig. 7. The L_2 norm of absolute errors on different meshes for the Couette flow at Kn = 0.1. The slope of the fitting line is about 1.91.

2.3. Boundary condition

In UGKS, ghost cells are usually employed for imposing the boundary conditions. In implicit schemes for steady state solutions, for simplicity, the boundary conditions can be implemented in an explicit way as that in [35], where the flow variables in the ghost cells are directly derived from these in the corresponding inner cells, and the quantities in the delta-form in ghost cells are set to zero. In the framework of implicit schemes, the utilization of iterations to solve the matrix system in which the governing equations of the boundaries are included could lead to a truly implicit boundary treatment [36], which could slightly improve the convergence efficiency. In the following, the boundary conditions are implemented implicitly on the linearized relation between inner and ghost cells. Indeed, during the Gauss–Seidel iterations in solving the lower and upper triangular matrices, the delta-form quantities in ghost cells can be set explicitly. Moreover, with the LU-SGS technique, the implicit boundary conditions can be imposed by only one sweep process.

Generally, the relation between the conservative flow variables in the ghost cell j and the inner cell i can be expressed in the following form

$$\vec{W}_j = \vec{B}\left(\vec{W}_i\right), \tag{26}$$

where $\vec{B}$ represents a specific transformation relation. The linearization of the above equation gives

$$\Delta\vec{W}_j^{n+1} - \left(\frac{\partial\vec{B}}{\partial\vec{W}}\right)_i^n \Delta\vec{W}_i^{n+1} = \vec{0}, \tag{27}$$

which is the macroscopic governing equation of boundary conditions adopted in the prediction step of the implicit UGKS. For example, for a solid wall moving with velocity $\vec{U}_w = (U_0, V_0)$, Eq. (26) gives

$$\begin{aligned} &\rho_j = \rho_i, \\ &m_j = 2\rho_i U_0 - m_i, \\ &n_j = 2\rho_i V_0 - n_i, \\ &p_j = p_i, \quad or \quad T_j = T_i. \end{aligned} \tag{28}$$

After linearization, the changes of the conservative variables in the ghost cell vary with the values in the inner cell by

$$\begin{bmatrix} \Delta\rho_j \\ \Delta m_j \\ \Delta n_j \\ \Delta\varepsilon_j \end{bmatrix} = \begin{bmatrix} 1 & 0 & 0 & 0 \\ 2U_0 & -1 & 0 & 0 \\ 2V_0 & 0 & -1 & 0 \\ 2\left(U_0^2+V_0^2\right) & -2U_0 & -2V_0 & 1 \end{bmatrix} \begin{bmatrix} \Delta\rho_i \\ \Delta m_i \\ \Delta n_i \\ \Delta\varepsilon_i \end{bmatrix}. \tag{29}$$

Adding the boundary condition of Eq. (27) into the penta-diagonal matrix system, shown in Fig. 1(b), the matrix will keep the penta-diagonal form. Let's define L_{gc} for the set of ghost cells at the southern and western boundaries shown in Fig. 2(a),

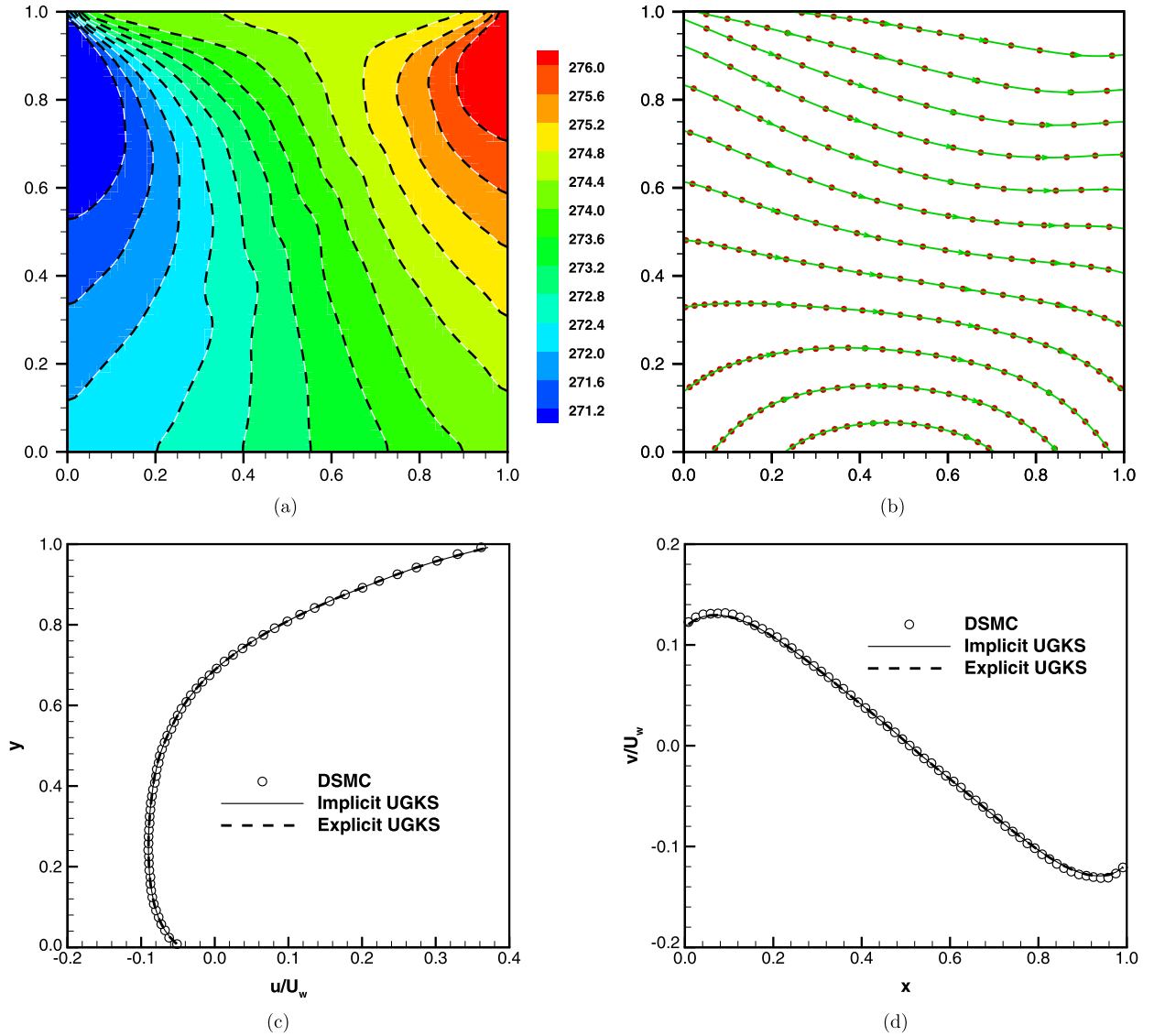

Fig. 8. Cavity flow at Knudsen number Kn = 10. (a) Temperature, background: implicit UGKS, dashed line: explicit UGKS; (b) heat flux, circle: explicit UGKS, line with arrowhead: implicit UGKS; (c) u-velocity along the central vertical line and (d) v-velocity along the central horizontal line.

and U_{gc} as the ghost cells at the northern and eastern boundaries shown in Fig. 2(b). The boundary conditions related to the ghost cells $j \in L_{gc}$ and $j \in U_{gc}$ will respectively appear in the lower and upper triangular region of the iterative matrix system. For LU factorization method, it will always give $\Delta\vec{W}_j = \vec{0}$ for the ghost cells $j \in L_{gc}$, and $\Delta\vec{W}_j = \left(\partial\vec{B}/\partial\vec{W}\right)_i \Delta\vec{W}_i$ for the ghost cells $j \in U_{gc}$. Thus with LU-SGS technique, the Gauss–Seidel iterations could initialize the ghost cells $j \in L_{gc}$ explicitly with the condition,

$$\Delta\vec{W}_j|_{j\in L_{gc}} = \vec{0},$$

in the forward sweep step, and set the ghost cells $j \in U_{gc}$ explicitly with the condition,

$$\Delta\vec{W}_j|_{j\in U_{gc}} = \left(\partial\vec{B}/\partial\vec{W}\right)_i \Delta\vec{W}_i,$$

in the backward sweep step. In addition, for the PR(m) scheme, during inner iterations Eq. (27) will be implemented in all ghost cells with the conservative flow variables $\Delta\vec{W}_i^{m-1}$ updated from the $(m-1)$-th sweep step.

The boundary conditions for the gas distribution function in the evolution step of the implicit UGKS could be done similarly. However, it is not easy to find such a simple relation of Eq. (26) between distribution function $f_{j,k}$ and $f_{i,k}$ for each velocity point. Therefore, only a few specific types of boundaries for the distribution function will be discussed.

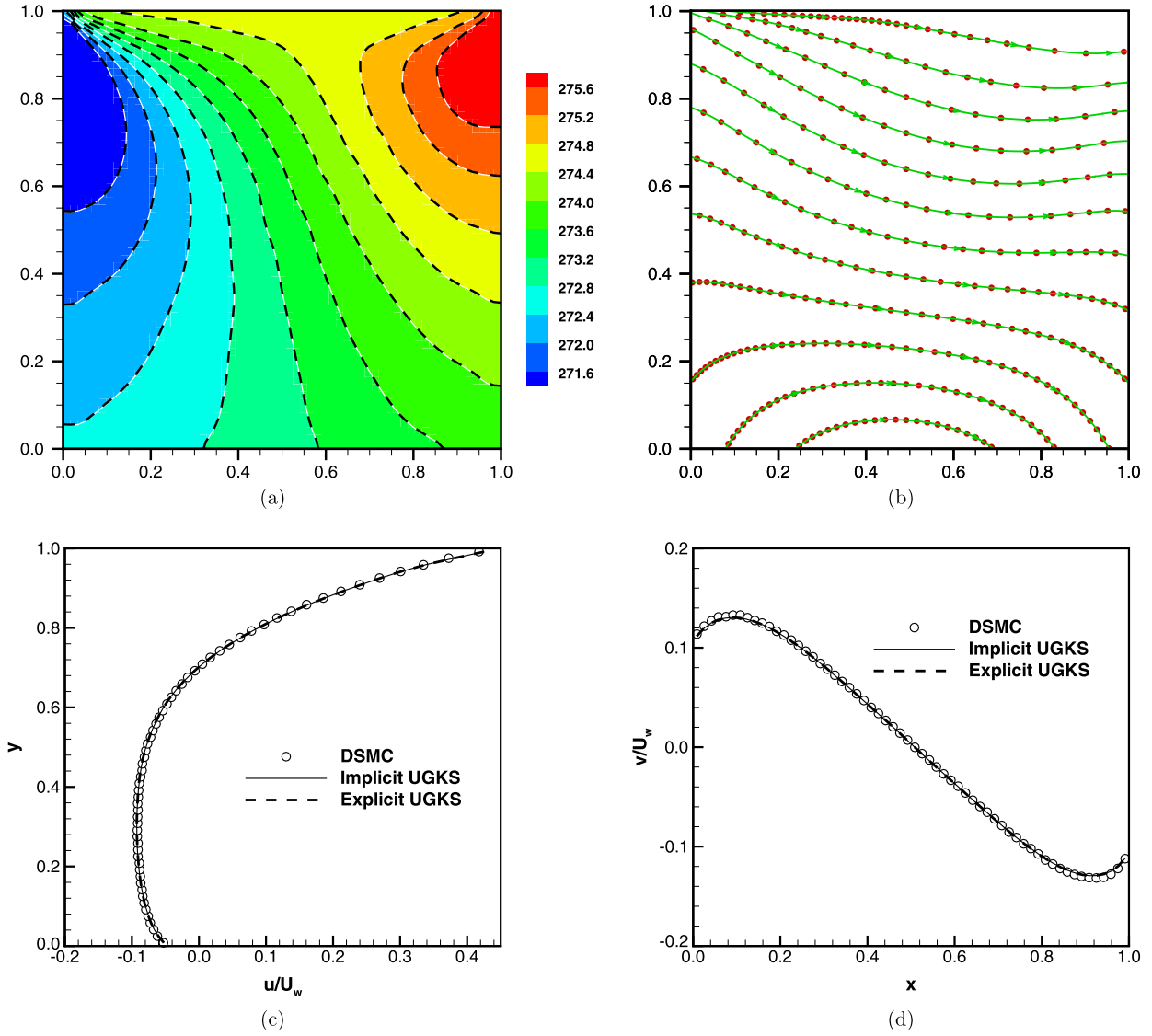

Fig. 9. Cavity flow at Knudsen number Kn = 1.0. (a) Temperature, background: implicit UGKS, dashed line: explicit UGKS; (b) heat flux, circle: explicit UGKS, line with arrowhead: implicit UGKS; (c) u-velocity along the central vertical line and (d) v-velocity along the central horizontal line.

(1) Symmetric boundary. For a symmetric boundary shared by the ghost cell j and the inner cell i, obviously we have $f_{j,k} = f_{i,k'}$ where the discretized velocities $\vec{u}_k$ and $\vec{u}_{k'}$ are symmetric with respect to this boundary. Then, we have $\Delta f_{j,k} = \Delta f_{i,k'}$.
(2) Inlet condition for supersonic flows and flow at far fields. In these cases, for simplicity the distribution function could be regarded as Maxwellian distribution determined by the initial condition, i.e., $f_{j,k}$ is constant. The variation of the distribution function in each velocity space will keep to zero, i.e., $\Delta f_{j,k} = 0$.
(3) Outlet boundary. The distribution function in ghost cells is calculated by interpolation from inner cells, such as $f_{j,k} = f_{i,k}$ or $f_{j,k} = af_{i,k} + bf_{i-1,k} + \cdots$. Then, we have $\Delta f_{j,k} = \Delta f_{i,k}$ or $\Delta f_{j,k} = a\Delta f_{i,k} + b\Delta f_{i-1,k} + \cdots$.

For an isothermal solid wall with moving velocity $\vec{U} = (U_w, V_w)$ and temperature T_w, for the diffusive reflection boundary condition the reduced distribution function in ghost cells is

$$f_{j,k} = \rho_j \cdot \frac{m_0}{2\pi k_B T_w} \exp\left\{-\frac{m_0}{2k_B T_w}\left[(u_k - U_w)^2 + (v_k - V_w)^2\right]\right\} = \rho_j \cdot C_k, \tag{30}$$

where all parameters at each discrete particle velocity k are fixed except ρ_j. Therefore, for a solid wall on the left, the variation of gas distribution functions in ghost cells are determined by

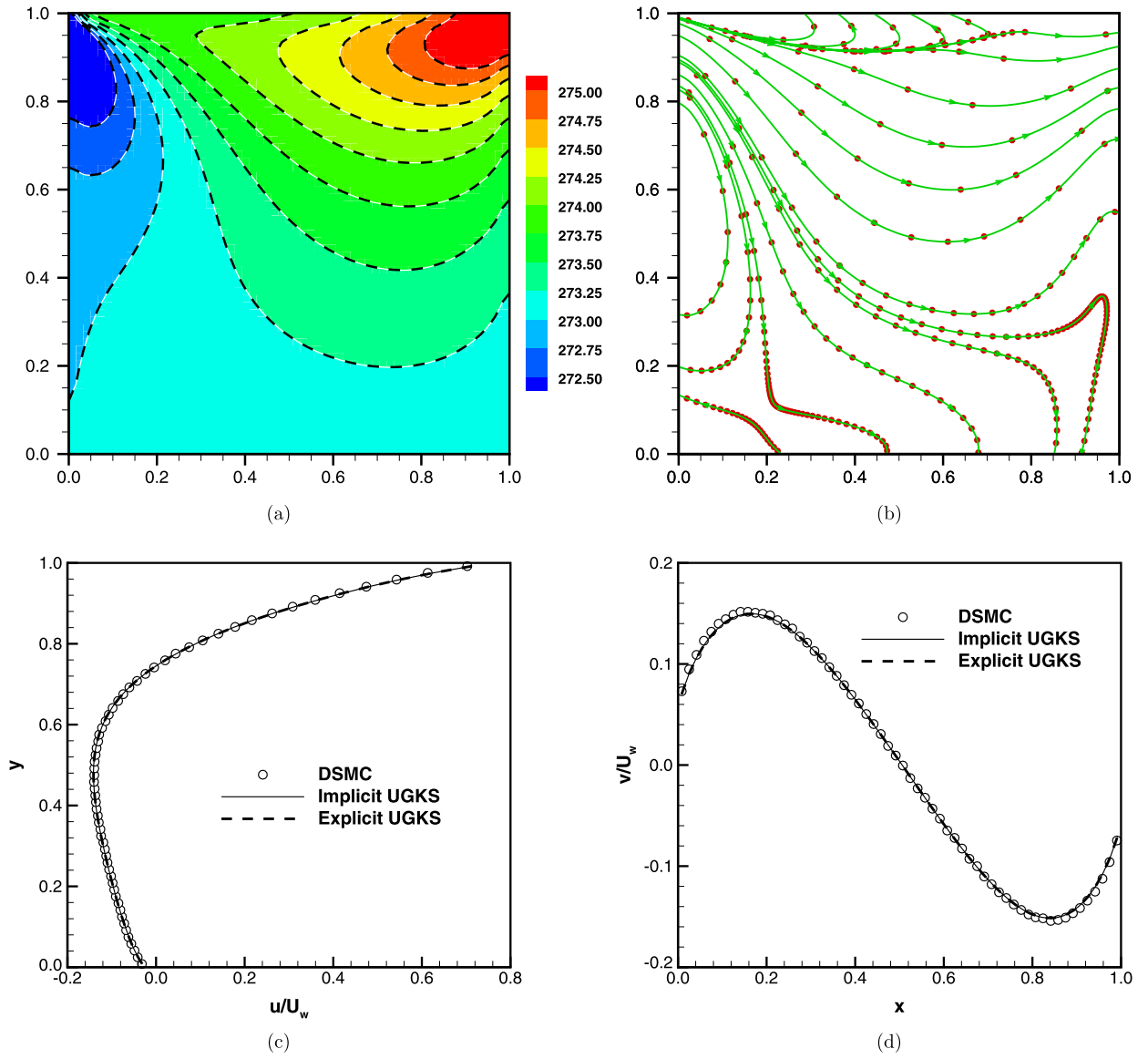

Fig. 10. Cavity flow at Knudsen number Kn = 0.075. (a) Temperature, background: implicit UGKS, dashed line: explicit UGKS; (b) heat flux, circle: explicit UGKS, line with arrowhead: implicit UGKS; (c) u-velocity along the central vertical line and (d) v-velocity along the central horizontal line.

$$\Delta f_{j,k} = \Delta \rho_j \cdot C_k, \tag{31}$$

where $\Delta \rho_j$ is computed by no-transmission condition

$$\Delta \rho_j \int_{u_n<0} u_n \frac{m_0}{2\pi k_B T_w} \exp\{-\frac{m_0}{2k_B T_w}\left[(u-U_w)^2+(v-V_w)^2\right]\} du dv = -\sum_{u_{n,k}>0} u_{n,k} \Delta f_{i,k}. \tag{32}$$

Once the relation between Δf_j and Δf_i is constructed, the forward sweep could begin with the condition $\Delta f_{j,k} = 0$ in ghost cells $j \in L_{gc}$. The boundary condition $\Delta f_{j,k}$ computed from Δf_i can be used directly in the backward sweep step for the ghost cells $j \in U_{gc}$.

2.4. Remarks on the implicit scheme

In order to improve the acceleration efficiency of the implicit scheme, especially for continuum and near continuum flows, a prediction step is introduced in Section 2.2.1 to determine the equilibrium state. Two iteration methods, i.e., the LU-SGS method in Eq. (16) and (17), and the point relaxation scheme in Eq. (18) and (19), have been presented in order

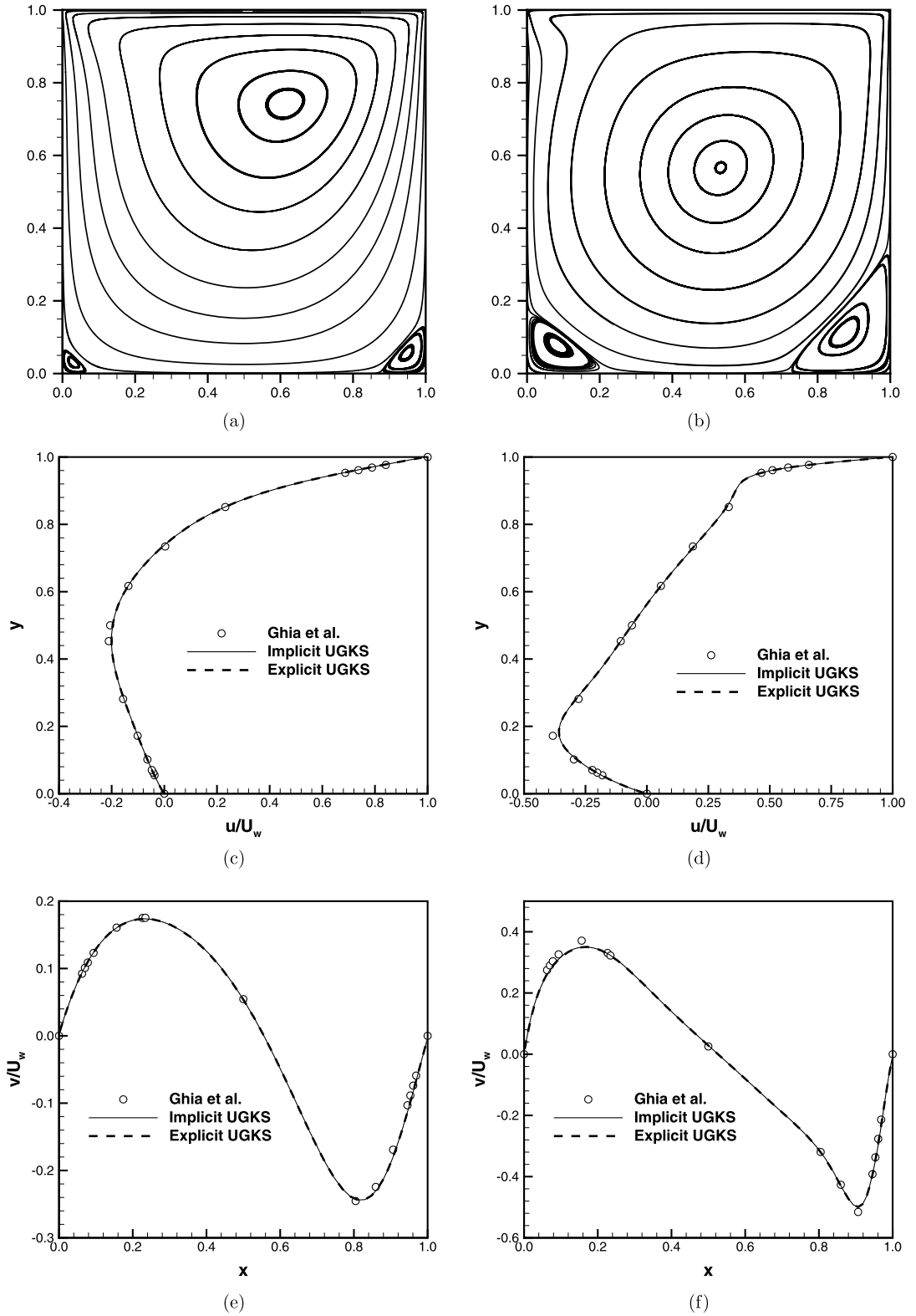

Fig. 11. Cavity flows at Reynolds number Re = 100 (left) and Re = 1000 (right). (a) and (b) Streamlines; (c) and (d) u-velocity along the central vertical line; (e) and (f) v-velocity along the central horizontal line. Circle denotes the data obtained from [41].

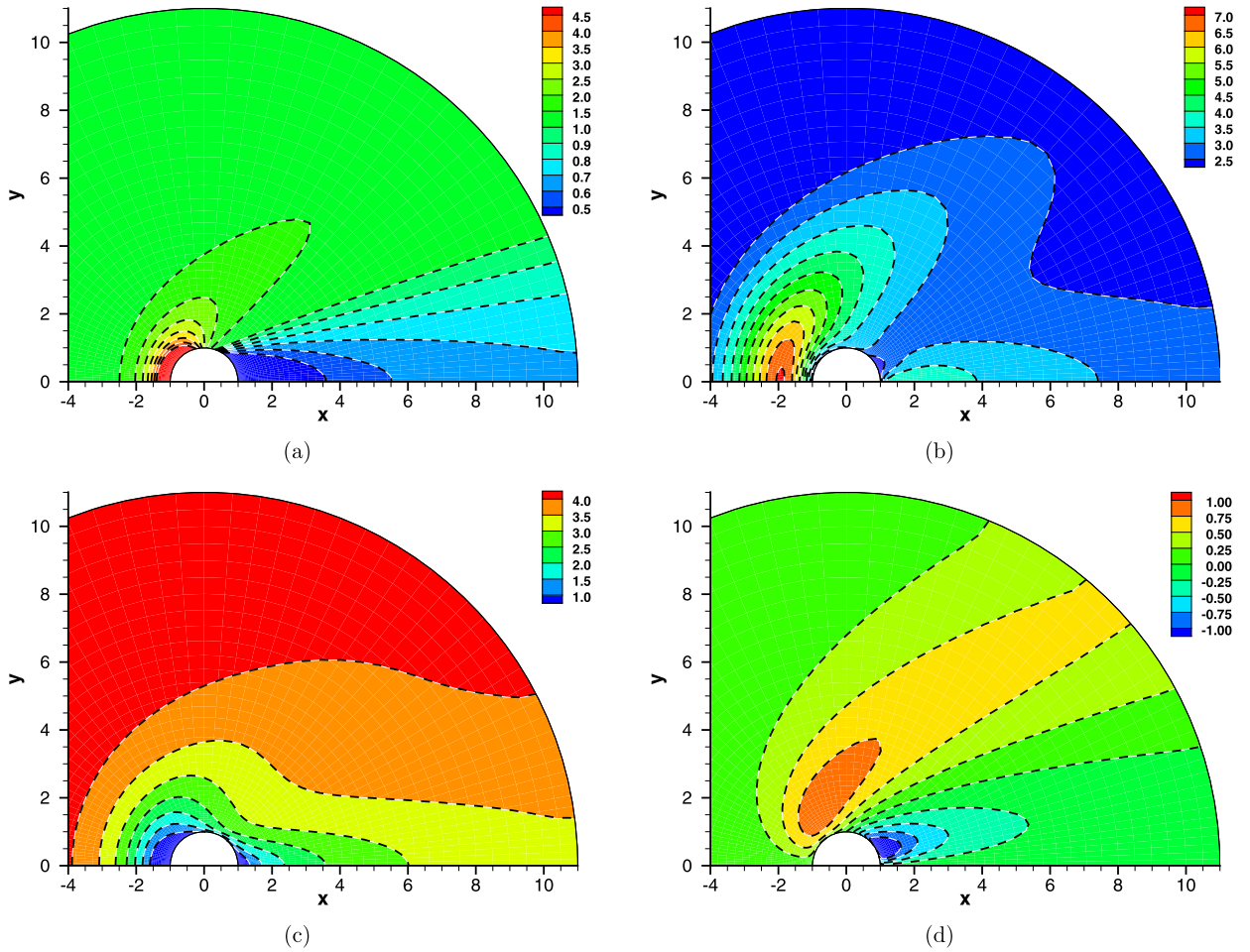

Fig. 12. Flow contours around a cylinder at $\mathrm{Kn} = 1$ and $\mathrm{Ma}_\infty = 5$. (a) Density; (b) temperature; (c) U-velocity and (d) V-velocity. Background: the explicit solution; dashed line: the implicit solution.

Table 3
Efficiency and accuracy of the implicit UGKS for cavity flow.

State	Explicit UGKS		Implicit UGKS			
	Steps	Time (s)	Steps	Time (s)	Rate	Error (%)
$\mathrm{Kn} = 10$	9082	35 249	205	1030	34.2	1.100
$\mathrm{Kn} = 1$	4089	12 099	188	721	16.8	0.580
$\mathrm{Kn} = 0.075$	7005	10 575	197	386	27.4	0.030
$\mathrm{Re} = 100$	357 369	169 391	1443	868	195.1	0.002
$\mathrm{Re} = 1000$	843 234	402 552	3378	1971	204.2	−0.07

to solve the macroscopic equations implicitly. In order to distinguish these two approaches, these two implicit methods are defined as the implicit UGKS (A) and the implicit UGKS (B). The performance of these two methods will be evaluated in the next section.

In Eq. (13), the term in front of $\Delta \vec{W}_i^{n+1}$ will reside in the principal diagonal of the penta-matrix, as shown in Fig. 1. So, the numerical time step Δt and the parameter r_{ij} are closely correlated with the stability and convergence efficiency of the scheme. A simple analysis shows that a larger numerical time step will result in a faster convergence. When the numerical time step is large enough, the convergence will depend only on the calculation of r_{ij}. This parameter can be computed by Eq. (12) with a stable factor s_{ij}, or by $r_{ij} = \varpi \Lambda_{ij}$ with an over-relaxation parameter. A larger r_{ij} may increase the stability of the scheme, but could decrease the convergence efficiency. An adjustable over-relaxation parameter ϖ will be helpful to balance the convergence efficiency and the stability of the scheme. In the present paper, the over-relaxation parameter ϖ is set to be one.

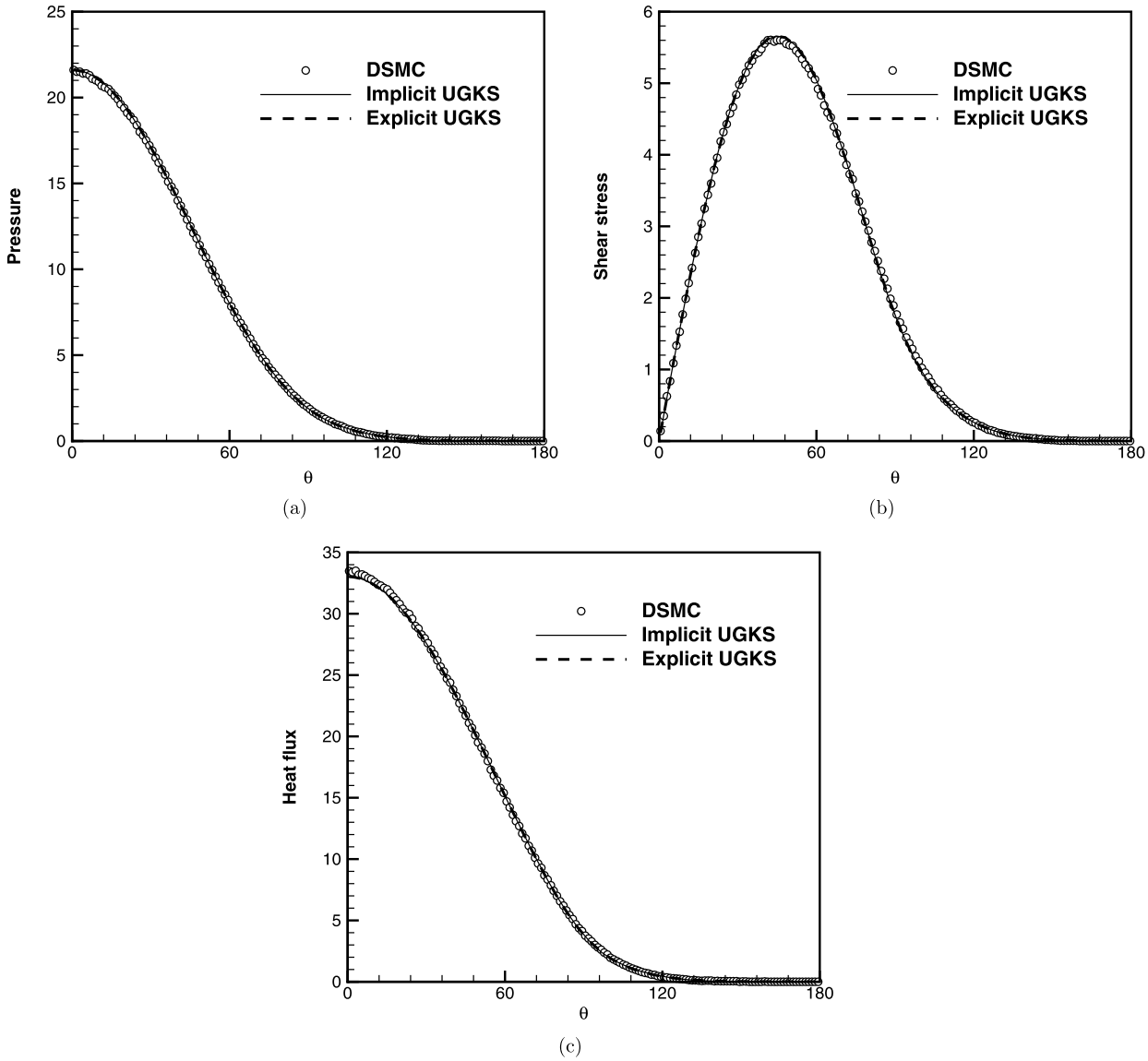

Fig. 13. Flow variables along the surface of the cylinder for the case of $\mathrm{Kn} = 1$ and $\mathrm{Ma}_\infty = 5$. (a) Pressure; (b) shear stress and (c) heat flux.

Since residuals on the right hand sides of Eq. (13) and (22) in the implicit UGKS are completely calculated by the explicit UGKS, the solutions obtained from the implicit scheme and the explicit scheme will be identical for a steady state solution. Although Eq. (13) and (20) are based on the Euler backward method with a first-order accuracy in time, the implicit UGKS is still of second-order accuracy for steady flow solution, because the residual is fully controlled by the explicit UGKS flux with second-order accuracy.

The LU factorization method may introduce some errors related to the numerical time step Δt in the implicit system. It is also realized that the Gauss–Seidel iteration during sweep steps may not be so physical because the flux flowing out of one cell may not be totally equal to the flux received by its neighboring cells. Moreover, due to the utilization of the most recent values in the Gauss–Seidel iteration, the solution of each cell is not strictly evaluated at the same time level during the sweep steps. In the numerical examples, it is found that for an opening system the convergent solution from the implicit UGKS is fully consistent with solution of the explicit scheme, because the supplement at far field boundary can automatically remedy any error mentioned above. For a closed system, the implicit scheme can still give a convergent solution, but may have losses or gains of flow quantities, such as the mass. Fortunately, the results are not deteriorated too much from the implicit iterations. Technically, since the total mass in a closed system is known, this problem can be fully solved by proportionally adjusting the conservative flow variables and distribution function during the iterations. Some other factors which would influence the accuracy and the convergence efficiency of the implicit scheme, such as iteration methods in prediction step and numerical time step, will be discussed specifically in the numerical examples.

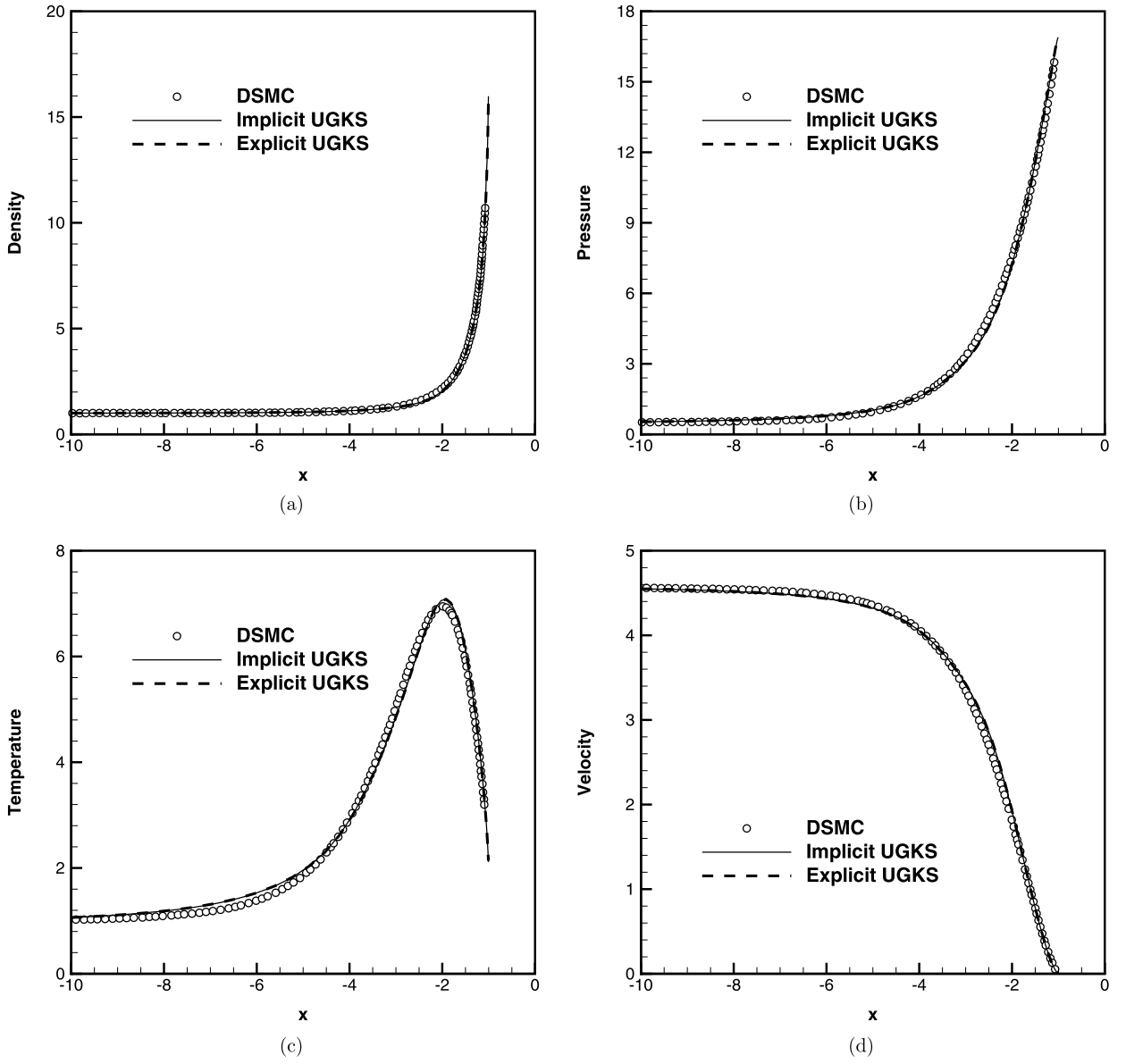

Fig. 14. Flow variables along the central symmetric line for the case of $\mathrm{Kn} = 1$ and $\mathrm{Ma}_\infty = 5$. (a) Density; (b) pressure; (c) temperature and (d) velocity.

3. Numerical experiments

In this section, the Couette flow, lid-driven cavity flow, and supersonic flow passing over a circular cylinder, will be used to validate the implicit UGKS. All numerical simulations are conducted on a personal computer with Intel(R) Core(TM) i5-4570 CPU @ 3.2 GHz.

3.1. Couette flow

The Couette flow is driven by two parallel plates moving in opposite directions with velocity U_w, see Fig. 3. The Knudsen number is defined as the ratio of mean free path to the distance H between two plates. The physical space between two plates is discretized with 100 cells. The physical time step used in the implicit scheme is determined by the CFL condition with a CFL number 0.8.

The velocity distributions along y-direction are plotted in Fig. 4 for different Knudsen numbers. In transition regime and free molecular regime, the solutions of IP method [37] are used as references. For the cases at Knudsen numbers $\mathrm{Kn} = 0.2/\sqrt{\pi}, 2.0/\sqrt{\pi}$, and $20/\sqrt{\pi}$, the wall velocity is set to be $U_w = 0.5\sqrt{RT_w}$ and 80×80 points in velocity space are used. In slip regime, another Knudsen number $\mathrm{Kn} = 0.01$ case is calculated and its solution is compared with the

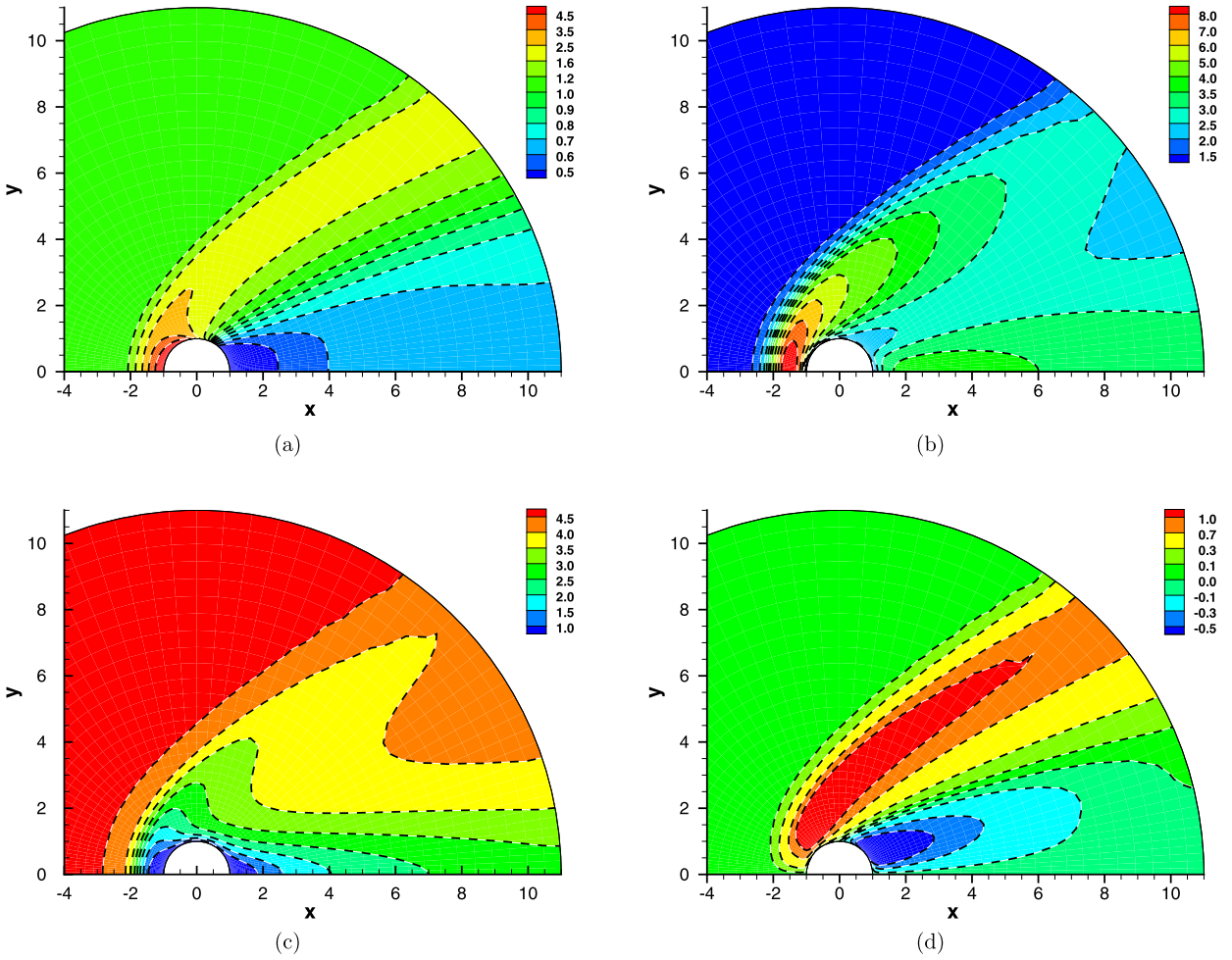

Fig. 15. Flow contours around a cylinder at $\mathrm{Kn} = 0.1$ and $\mathrm{Ma}_\infty = 5$. (a) Density; (b) temperature; (c) U-velocity and (d) V-velocity. Background: the explicit solution; dashed line: the implicit solution.

data in [38]. Furthermore, the Couette flow at $\mathrm{Kn} = 10^{-4}$ with $U_w = 0.1\sqrt{RT_w}$ is simulated to validate the implicit UGKS in continuum limit. The discrete points in velocity space can be much reduced in the continuum flow limit. Here, the Gauss–Hermite quadrature with 28×28 velocity points is utilized. Fig. 4(b) shows solutions from both implicit and explicit schemes, as well as the analytical NS solutions. Fig. 5 shows the calculated stress in the whole flow regime in comparison with reference solutions [39].

In general, in comparison with the explicit UGKS, the implicit scheme can increase the convergence rate by one or two orders of magnitude in different flow regimes. Detailed results are given in Table 1. For the implicit scheme, in the rarefied regime the sweep process and the upwind method in Eq. (21) speed up the numerical information propagation and accelerate the convergence. In the continuum flow regime, the prediction step of macroscopic equations for the evaluation of equilibrium state plays an important role for the convergence. For the flow between the above two limits, the convergent rate is not accelerated too much. This is mainly due to the fact that the above two acceleration mechanism for the rarefied (micro) and continuum (macro) has limited effect in the intermediate regime, but a speed-up of 20 times is still significant. The mass loss is also given in Table 1, which is acceptable.

In order to further explore the effects of the prediction step and the numerical time step on the convergence, the implicit UGKS (A) and UGKS (B) are compared with a reference implicit scheme without prediction step [26], where the equilibrium state $\tilde{g}^{n+1}$ is simply approximated by g^n. The comparison is listed in Table 2. In the comparison, the steady state is defined by the L_2 norm of the residuals $\vec{R}_i^n$, which is smaller than 1.0×10^{-10} for convergence. The time evolutions of residual of different schemes with $\mathrm{CFL} = 10$ and $\mathrm{CFL} = 10\,000$ are plotted in Fig. 6. The overall convergence efficiency increases 167% for the implicit UGKS (A) and 279% for the implicit UGKS (B) in comparison with the reference implicit method. It shows that the prediction step does make contribution to improve convergence efficiency, and this effect will become more obvious for the continuum and near continuum flow computations. With the increment of numerical time step, the efficiency can be

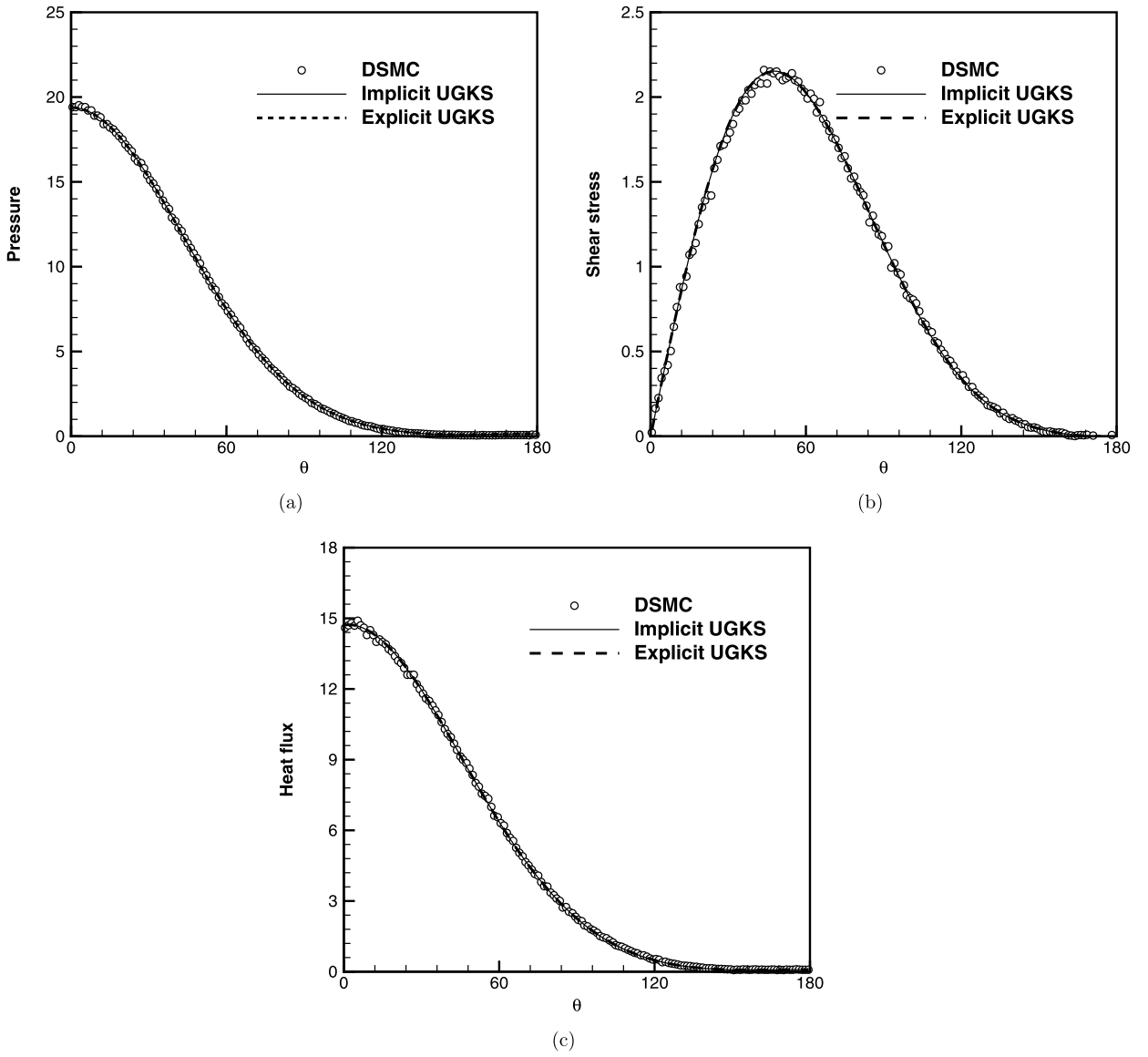

Fig. 16. Flow variables along the surface of the cylinder for case of $\mathrm{Kn} = 0.1$ and $\mathrm{Ma}_\infty = 5$. (a) Pressure; (b) shear stress and (c) heat flux.

improved up to a maximum value. Based on the solution at $\mathrm{Kn} = 0.1$, accuracy of the implicit UGKS is tested. The error in L_2 norm with respect to mesh size is plotted in Fig. 7, which shows a second-order accuracy of the implicit scheme.

3.2. Cavity flow

The lid-driven cavity flows are studied at different Knudsen numbers. The cavity has a fixed wall temperature $T_w = 273$ K. The gas inside cavity is argon with mass $m_0 = 6.63 \times 10^{-26}$ kg. The Kundsen number is defined as the ratio of mean free path to the length of cavity side wall, and the mean free path of gas is evaluated for a hard sphere model. Following the previous studies [29,40], the wall velocity is $U_w = 50$ m/s for cases at $\mathrm{Kn} = 10$, 1.0 and 0.075. In continuum flow limit at $\mathrm{Re} = 100$ and 1000 with corresponding $\mathrm{Kn} = 1.44 \times 10^{-3}$ and $\mathrm{Kn} = 5.42 \times 10^{-4}$, the solutions are compared with the NS ones [41]. In order to compare with DSMC results, the dynamic viscosity used in the implicit UGKS is given by $\mu = \mu_{ref}(T/T_{ref})^{\omega}$ with $\omega = 0.81$.

The computational domain is discretized using a mesh of 61×61 cells in physical space. For continuum flow, the mesh is stretched to get a better resolution near the boundaries, where the size of the finest cell is about 0.004×0.004. The particle velocity points are 80×80, 70×70 and 50×50 for the flows at $\mathrm{Kn} = 10$, 1.0 and 0.075. The trapezoidal integration is used to compute the moments of the distribution function in these cases. Gauss–Hermite quadrature with 28×28 points

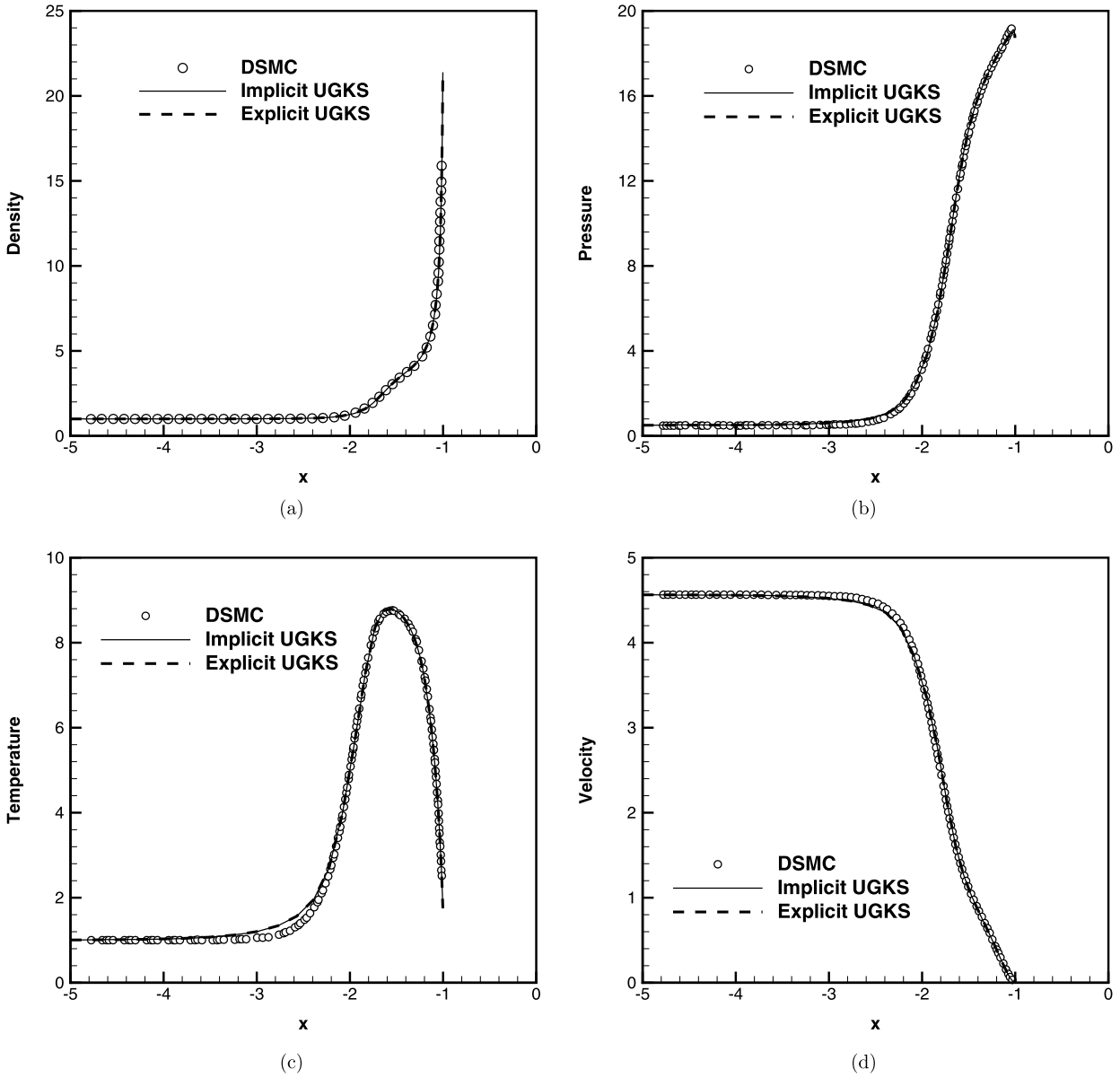

Fig. 17. Flow variables along the central symmetric line for the case of $\mathrm{Kn} = 0.1$ and $\mathrm{Ma}_\infty = 5$. (a) Density; (b) pressure; (c) temperature and (d) velocity.

in velocity space is adopted for continuum flow cases at $\mathrm{Re} = 100$ and 1000. The time step used in explicit UGKS and the physical time step in the implicit one are both based on the CFL condition with $\mathrm{CFL} = 0.8$.

Results at $\mathrm{Kn} = 10$, 1 and 0.075 are presented in Figs. 8, 9, and 10, where the temperature contours, heat flux, and velocity along the central line are shown. Excellent results are obtained from the implicit UGKS. The streamlines at Reynolds numbers $\mathrm{Re} = 100$ and 1000 are plotted in Fig. 11. The acceleration rate and mass loss of the implicit scheme in different flow regimes are listed in Table 3, in which the data are obtained at the residual of 1.0×10^{-9}.

3.3. Cylinder flow

The supersonic flow passing over a circular cylinder at Knudsen numbers $\mathrm{Kn} = 1.0$ and $\mathrm{Kn} = 0.1$ (with respect to cylinder radius) are computed. The monatomic argon gas with molecule mass $m_0 = 6.63 \times 10^{-26}$ kg at a velocity $U_\infty = 1538.7$ m/s or Mach number $\mathrm{Ma}_\infty = 5$ hits on the cylinder. The free stream has a temperature $T_\infty = 273$ K. The variable hard sphere model with a reference diameter $d_0 = 4.17 \times 10^{-10}$ m is used in the calculation. The cylinder has a cold solid wall with a fixed temperature $T_w = 273$ K. The physical domain is discretized by a mesh with 50×64 cells, and the velocity space has

90×90 mesh points. Diffusive reflection boundary condition is used on the isothermal wall. The physical time step in the implicit scheme is computed by the CFL condition with CFL number 0.5.

The steady state solutions at $\mathrm{Kn} = 1$ and $\mathrm{Kn} = 0.1$ are presented in Fig. 12 and Fig. 15, in which the density, temperature, and velocity contours are plotted and compared with the results from the explicit UGKS. The flow variables along the surface of the cylinder are shown in Fig. 13 and Fig. 16, which are compared with the DSMC solutions [29]. The distributions of density, pressure, temperature, and velocity along the symmetric axis in front of the cylinder are also plotted in Fig. 14 and Fig. 17. Generally, the results from the implicit scheme agree well with the DSMC and explicit UGKS solutions. In terms of efficiency, the implicit UGKS can get the steady state solution within two hours, but it will take about 4 days at $\mathrm{Kn} = 1.0$ and one week at $\mathrm{Kn} = 0.1$ for the explicit UGKS to reduce the residual to the order of 10^{-4} and 10^{-5} by using a personal computer with Intel(R) Core(TM) i5-4570 CPU @ 3.2 GHz. The overall efficiency is increased by one and two orders of magnitude.

4. Conclusions

In this paper, an implicit unified gas-kinetic scheme is constructed for the steady state solution in all flow regimes. Since the physics represented in the UGKS depends on the time step, in order to capture the multiscale solution, a physical and a numerical time steps are used in the implicit UGKS. As a result, accurate solutions have been obtained from implicit UGKS in all flow regimes. Since the UGKS has governing equations for both macroscopic flow variables and microscopic gas distribution function, the use of the coupled implicit macroscopic and microscopic iterative equations increases the efficiency of the scheme greatly, especially in the highly non-equilibrium and in the near continuum limits. Two iterative methods are used in the prediction step, which are the LU-SGS method and the point relaxation scheme.

The numerical tests of Couette flow, cavity flow, and flow passing over a cylinder, validate the current implicit method. The influence of numerical time step and the iteration methods in the prediction step on the convergence rate are quantitatively evaluated. Due to the delta-form formulations in Eq. (13) and (20), the implicit UGKS can get the same steady state solution as that of the explicit UGKS, and the implicit scheme has the same second-order accuracy as the explicit one. The implicit scheme for a two dimensional case takes 50.4% more memory and 26.3% more computational time for the update of each step than the explicit scheme. But, the implicit UGKS can improve the convergence rate by one or two orders of magnitude. For steady state computation, many other accelerating techniques, such as parallel computing, local time stepping, and multigrid technique, have been well developed in the past decades in the computational fluid dynamics community. But these methods have not been employed in the present study. So, there is still space for the further improvement of the efficiency of UGKS. In comparison with particle-based DSMC method, the UGKS has great potential for the flow study in all flow regimes once the advantages of equations-based numerical techniques can be fully explored.

Acknowledgements

This work of Zhu and Zhong was supported by National Natural Science Foundation of China (Grant No. 11472219) and National Pre-Research Foundation of China. The research of Xu was supported by Hong Kong research grant council (620813, 16211014, 16207715) and HKUST (PROVOST13SC01, IRS15SC29, SBI14SC11).

References

[1] P.L. Bhatnagar, E.P. Gross, M. Krook, A model for collision processes in gases. I. Small amplitude processes in charged and neutral one-component systems, Phys. Rev. 94 (3) (1954) 511–525.
[2] K.H. Prendergast, K. Xu, Numerical hydrodynamics from gas-kinetic theory, J. Comput. Phys. 109 (1) (1993) 53–66.
[3] K. Xu, K.H. Prendergast, Numerical Navier–Stokes solutions from gas kinetic theory, J. Comput. Phys. 114 (1) (1994) 9–17.
[4] K. Xu, A gas-kinetic BGK scheme for the Navier–Stokes equations and its connection with artificial dissipation and Godunov method, J. Comput. Phys. 171 (1) (2001) 289–335.
[5] S. Chapman, T.G. Cowling, The Mathematical Theory of Non-uniform Gases: An Account of the Kinetic Theory of Viscosity, Thermal Conduction and Diffusion in Gases, Cambridge University Press, 1970.
[6] K. Xu, J.-C. Huang, A unified gas-kinetic scheme for continuum and rarefied flows, J. Comput. Phys. 229 (20) (2010) 7747–7764.
[7] K. Xu, Direct Modeling for Computational Fluid Dynamics: Construction and Application of Unified Gas-Kinetic Schemes, World Scientific, Singapore, 2015.
[8] S. Chen, K. Xu, A comparative study of an asymptotic preserving scheme and unified gas-kinetic scheme in continuum flow limit, J. Comput. Phys. 288 (2015) 52–65.
[9] C. Liu, K. Xu, Q. Sun, Q. Cai, A unified gas-kinetic scheme for continuum and rarefied flows IV: full Boltzmann and model equations, J. Comput. Phys. (2016), http://dx.doi.org/10.1016/j.jcp.2016.03.014.
[10] W. Sun, S. Jiang, K. Xu, An asymptotic preserving unified gas kinetic scheme for gray radiative transfer equations, J. Comput. Phys. 285 (2015) 265–279.
[11] G.A. Bird, Molecular Gas Dynamics and the Direct Simulation of Gas Flows, Oxford University Press, USA, 1994.
[12] L. Mieussens, Discrete-velocity models and numerical schemes for the Boltzmann–BGK equation in plane and axisymmetric geometries, J. Comput. Phys. 162 (2) (2000) 429–466.
[13] L. Mieussens, Discrete velocity model and implicit scheme for the BGK equation of rarefied gas dynamics, Math. Models Methods Appl. Sci. 10 (08) (2000) 1121–1149.
[14] Z.-H. Li, L. Bi, H.-X. Zhang, L. Li, Gas-kinetic numerical study of complex flow problems covering various flow regimes, Comput. Math. Appl. 61 (12) (2011) 3653–3667.
[15] D. Chae, C. Kim, O.-H. Rho, Development of an improved gas-kinetic BGK scheme for inviscid and viscous flows, J. Comput. Phys. 158 (1) (2000) 1–27.

[16] S. Yoon, A. Jameson, A Multigrid LU-SSOR Scheme for Approximate Newton Iteration Applied to the Euler Equations, National Aeronautics and Space Administration, 1986.
[17] A. Jameson, S. Yoon, Lower–upper implicit schemes with multiple grids for the Euler equations, AIAA J. 25 (7) (1987) 929–935.
[18] S. Yoon, A. Jameson, Lower–upper symmetric-Gauss–Seidel method for the Euler and Navier–Stokes equations, AIAA J. 26 (9) (1988) 1025–1026.
[19] H. Rieger, A. Jameson, Solution of steady three-dimensional compressible Euler and Navier–Stokes equations by an implicit LU scheme, in: AIAA, Aerospace Sciences Meeting, 26th, Reno, NV, 1988.
[20] D. Sharov, K. Nakahashi, Reordering of 3-D hybrid unstructured grids for vectorized LU-SGS Navier–Stokes computations, in: AIAA Paper 97, 1997, pp. 2102–2117.
[21] K. Xu, M. Mao, L. Tang, A multidimensional gas-kinetic BGK scheme for hypersonic viscous flow, J. Comput. Phys. 203 (2) (2005) 405–421.
[22] Q. Li, S. Fu, Applications of implicit BGK scheme in near-continuum flow, Int. J. Comput. Fluid Dyn. 20 (6) (2006) 453–461.
[23] J. Jiang, Y. Qian, Implicit gas-kinetic BGK scheme with multigrid for 3D stationary transonic high-Reynolds number flows, Comput. Fluids 66 (2012) 21–28.
[24] W. Li, M. Kaneda, K. Suga, An implicit gas kinetic BGK scheme for high temperature equilibrium gas flows on unstructured meshes, Comput. Fluids 93 (2014) 100–106.
[25] J. Yang, J. Huang, Rarefied flow computations using nonlinear model Boltzmann equations, J. Comput. Phys. 120 (2) (1995) 323–339.
[26] M. Mao, D. Jiang, J. Li, et al., Study on implicit implementation of the unified gas kinetic scheme, Chin. J. Theor. Appl. Mech. 47 (5) (2015) 822–829.
[27] W.T. Taitano, D.A. Knoll, L. Chacón, J.M. Reisner, A.K. Prinja, Moment-based acceleration for neutral gas kinetics with BGK collision operator, J. Comput. Theor. Transp. 43 (1–7) (2014) 83–108.
[28] E. Shakhov, Generalization of the Krook kinetic relaxation equation, Fluid Dyn. 3 (5) (1968) 95–96.
[29] J.-C. Huang, K. Xu, P. Yu, A unified gas-kinetic scheme for continuum and rarefied flows II: multi-dimensional cases, Commun. Comput. Phys. 12 (3) (2012) 662–690.
[30] J. Blazek, Computational Fluid Dynamics: Principles and Applications, Elsevier, 2001.
[31] S. Yoon, D. Kwakt, Implicit Navier–Stokes solver for three-dimensional compressible flows, AIAA J. 30 (11) (1992) 2653–2659.
[32] R. Chen, Z. Wang, Fast, block lower–upper symmetric Gauss–Seidel scheme for arbitrary grids, AIAA J. 38 (12) (2000) 2238–2245.
[33] S.E. Rogers, Comparison of implicit schemes for the incompressible Navier–Stokes equations, AIAA J. 33 (11) (1995) 2066–2072.
[34] L. Yuan, Comparison of implicit multigrid schemes for three-dimensional incompressible flows, J. Comput. Phys. 177 (1) (2002) 134–155.
[35] L. Zhang, Z. Wang, A block LU-SGS implicit dual time-stepping algorithm for hybrid dynamic meshes, Comput. Fluids 33 (7) (2004) 891–916.
[36] K. Aoki, P. Degond, L. Mieussens, et al., Numerical simulations of rarefied gases in curved channels: thermal creep, circulating flow, and pumping effect, Commun. Comput. Phys. 6 (5) (2009) 919.
[37] J. Fan, C. Shen, Statistical simulation of low-speed rarefied gas flows, J. Comput. Phys. 167 (2) (2001) 393–412.
[38] W. Marques Jr., G. Kremer, F. Sharipov, Couette flow with slip and jump boundary conditions, Contin. Mech. Thermodyn. 12 (6) (2000) 379–386.
[39] Y. Sone, S. Takata, T. Ohwada, Numerical analysis of the plane Couette flow of a rarefied gas on the basis of the linearized Boltzmann equation for hard-sphere molecules, Eur. J. Mech. B, Fluids 9 (1990) 273–288.
[40] B. John, X.-J. Gu, D.R. Emerson, Effects of incomplete surface accommodation on non-equilibrium heat transfer in cavity flow: a parallel DSMC study, Comput. Fluids 45 (1) (2011) 197–201.
[41] U. Ghia, K.N. Ghia, C. Shin, High-Re solutions for incompressible flow using the Navier–Stokes equations and a multigrid method, J. Comput. Phys. 48 (3) (1982) 387–411.